Selective Requirement for Polycomb Repressor Complex 2 in the Generation of Specific Hypothalamic Neuronal Sub-types

Behzad Yaghmaeian Salmani[1,2,#@], Brad Balderson[3@], Susanne Bauer[1], Helen Ekman[1], Annika Starkenberg[1], Thomas Perlmann[2], Michael Piper[4], Mikael Bodén[3] and Stefan Thor[1,4,$]

1) Department of Clinical and Experimental Medicine, Linkoping University, SE-58185, Linkoping, Sweden. 2) Department of Cell and Molecular Biology, Karolinska Institute, SE-171 65, Stockholm, Sweden. 3) School of Chemistry and Molecular Biosciences, and 4) School of Biomedical Sciences, University of Queensland, St Lucia QLD 4072, Australia.

Current addresses: #) Department of Cell and Molecular Biology, Karolinska Institute, SE-171 65, Stockholm, Sweden. $) School of Biomedical Sciences, University of Queensland, St Lucia QLD 4072, Australia

7 Figures
10 Supplemental Figures
11 Supplemental Tables

@ These authors contributed equally

Author for correspondence (ST): s.thor@uq.edu.au

Key words: Cell specification; epigenetics; H3K27me3; H3K36me3; neuropeptide neurons
Running title: PRC2 affects hypothalamus development

ABSTRACT

The hypothalamus displays staggering cellular diversity, chiefly established during embryogenesis by the interplay of several signalling pathways and a battery of transcription factors. However, the contribution of epigenetic cues to hypothalamus development remains unclear. We mutated the Polycomb Repressor Complex 2 gene *Eed* in the developing mouse hypothalamus, which resulted in the loss of H3K27me3; a fundamental epigenetic repressor mark. This triggered ectopic expression of posteriorly expressed regulators (e.g., Hox homeotic genes), upregulation of cell cycle inhibitors and reduced proliferation. Surprisingly, despite these effects, single cell transcriptomic analysis revealed that the majority of neuronal subtypes were still generated in *Eed* mutants. However, we observed an increase in Glutamatergic/GABAergic double-positive cells, as well as loss/reduction of dopamine, Hypocretin/Orexin and Tac2 neurons. These findings indicate that many aspects of the hypothalamic gene regulatory flow can proceed without the key H3K27me3 epigenetic repressor mark, and points to a unique sensitivity of particular neuronal sub-types to a disrupted epigenomic landscape.

INTRODUCTION

The hypothalamus is a small brain structure, which, in spite of its size acts as a master homeostatic regulator; controlling energy and fluid balance, thermoregulation, sleep-wake states, stress responses, growth and reproduction, as well as emotional and social behaviours (Saper and Lowell, 2014). The hypothalamus can perform this plethora of complex functions in large part due to its staggering neuronal diversity (Alpar et al., 2019; Romanov et al., 2019). Microarray and single cell transcriptomic analyses of the adult hypothalamus have resulted in major leaps in our understanding of the complete mature cellular diversity in this tissue, pointing to the presence of ~50 major cell types and several hundred subtypes (Campbell et al., 2017; Chen et al., 2017; Dalal et al., 2013; Henry et al., 2015; Jeong et al., 2016; Kim et al., 2019; Kurrasch et al., 2007; Lam et al., 2017; Mickelsen et al., 2019; Mickelsen et al., 2017; Moffitt et al., 2018; Romanov et al., 2017; Shimogori et al., 2010).

The development of the hypothalamus has been challenging to decode, not only due to its immense cellular diversity. Unlike other CNS regions, such as the cortex, hindbrain or spinal cord, which are arranged in columnar structures, the adult hypothalamus is characterized by a patchwork of partially overlapping nuclei and territories. Hypothalamic development is also characterized by complex tissue rearrangements and cellular migration (Bedont et al., 2015; Burbridge et al., 2016; Ferran et al., 2015; Puelles and Rubenstein, 2015). Despite these challenges, extensive efforts have resulted in the unravelling of a multi-step process of anterior-posterior and medio-lateral patterning events, involving many of the major signalling pathways (Shh, BMP, Nodal, WNT, FGF). This patterning process results in, and integrates with, the selective expression of a number of early transcription factors (TFs), which act to further sub-divide the hypothalamus. These early TFs in turn activate panels of late TFs within subdomains of the developing hypothalamus, which act with more restrictive mandates to specify diverse subsets of hypothalamic cell fates (Alvarez-Bolado, 2019; Bedont et al., 2015; Blackshaw et al., 2010; Burbridge et al., 2016; Ferran et al., 2015; Nesan and Kurrasch, 2016; Puelles and Rubenstein, 2015; Xie and Dorsky, 2017). More recently, single cell transcriptomic analysis of the embryonic hypothalamus has greatly increased our understanding of its developmental process (Huisman et al., 2019; Kim et al., 2020; Romanov et al., 2020; Zhang et al., 2021; Zhou et al., 2020).

In contrast to the identification of key signalling cues and TF pathways, the role of epigenetics in the control of hypothalamus development is not well understood. An intensively studied epigenetic regulator is the Polycomb Group complex (PcG), which is a collective name that refers to several different sub-complexes, where the Polycomb Repressor Complexes 1 and 2 (PRC1 and PRC2) are arguably most well-defined (Piunti and Shilatifard, 2016; Steffen and Ringrose, 2014). PRC2 mono-, di- and tri-methylates residue K27, chiefly on Histone 3.3, and to a lesser extent H3.2 and H3.1 (Banaszynski et al., 2013). In general, PRC2 triggers transcriptional repression of target genes, although its specific role in gene regulation and chromatin compaction is still under intensive investigation, an issue that is further challenged by the existence of variations in PRC2 protein complex composition (Chammas et al., 2020;

Laugesen et al., 2019; van Mierlo et al., 2019). In mammals, the *Embryonic ectoderm development* (*Eed*) gene constitutes a critical component of PRC2 and is encoded by a single gene in the mouse genome. *Eed* null mutants display an apparently complete loss of H3K27me1/2/3 (Montgomery et al., 2005), and when *Eed* is selectively removed in e.g., the hematopoietic lineage, in the intestine or in the CNS, H3K27me3 is lost (Jadhav et al., 2020; Xie et al., 2014; Yaghmaeian Salmani, 2018). Hence, in contrast to most, if not all other epigenetic marks and their enzyme systems, the single gene removal of *Eed* provides an unparalleled means of completely removing this key epigenetic mark.

To begin addressing the role of epigenetic input on hypothalamic development, we analysed *Eed* conditional mutants (*Eed-cKO*), where *Eed* was deleted by the early CNS deleter *Sox1-Cre*, which is active at E8.5 (Takashima et al., 2007). We find that *Eed-cKO* mutants display a complete loss of H3K27me3 in the hypothalamus, from E11.5 and onwards. *Eed-cKO* mutants upregulate several cell cycle inhibitor genes and display reduced proliferation in the hypothalamus. We also observed ectopic expression of many posteriorly expressed TFs, indicating posteriorization of the anterior CNS. To unravel the effects of *Eed-cKO* upon cell specification, we conducted single cell transcriptomic (scRNA-seq) analysis at E13.5, E15.5 and E18.5, spanning the major phase of hypothalamic cell specification (Kim et al., 2020; Romanov et al., 2020). Surprisingly, in spite of reduced proliferation and extensive ectopic TF expression, scRNA-seq analysis revealed that the majority of hypothalamic subtypes were generated in the *Eed-cKO* mutants. However, there was an increase in Glutamatergic/GABAergic double-positive cells, as well as loss/reduction of dopamine, Hypocretin/Orexin and a sub-group of Tac2 cells. scRNA-seq analysis revealed that these effects may result from dysregulation of several known cell-fate determinants. These findings suggest that many, but not all, aspects of the gene regulatory pathways necessary for hypothalamic development can play out irrespective of the H3K27me3 epigenetic mark, but points to higher sensitivity of certain neuronal sub-types to an altered epigenomic landscape.

RESULTS

Conditional knock out of *Eed* in the CNS results in the loss of H3K27me3

Constitutive *Eed* mutants die during early embryogenesis (Faust et al., 1998; Faust et al., 1995; Schumacher et al., 1996). To circumvent this early lethality we knocked out *Eed* conditionally in the CNS, by crossing a previously generated floxed *Eed* allele (Xie et al., 2014) to *Sox1-Cre* (Takashima et al., 2007). *Sox1* is expressed in the entire CNS and commences in the neural plate at E7.5 (Pevny et al., 1998). *Sox1-Cre* is a *Cre* insertion into the *Sox1* locus, and expresses *Cre* in agreement with the *Sox1* gene, as evident by Cre-mediated activation of a *ROSA26R-EYFP* reporter strain already at E8.5 in the entire developing CNS (Takashima et al., 2007). In contrast to *Eed* constitutive mutants, our conditional *Eed* mutants (denoted *Eed-cKO*) developed until at least E18.5. Hence, deleting *Eed* using *Sox1-Cre* circumvents early lethality while specifically removing *Eed* function from the entire developing hypothalamus at the earliest possible stage. We previously found that *Eed-cKO* embryos displayed loss of H3K27me3 immunostaining in the dorsal telencephalon and lumbo-sacral spinal cord, with a reduction of immunostaining at E10.5 and a complete loss at embryonic day E11.5 (Yaghmaeian Salmani et al., 2018). Focusing upon the developing hypothalamus we observed a loss of H3K27me3 immunostaining in the hypothalamus in *Eed-cKO* mutants, at E11.5 (Figure 1SA-J). Based upon these findings, and our previous study, we conclude that deletion of *Eed* by the early CNS-specific deleter *Sox1-Cre* results in loss of the H3K27me3 mark, albeit with a 2-3 day delay.

Eed-cKO mutants display reduced hypothalamic proliferation

Eed-cKO mutants display reduced proliferation in the dorsal telencephalon, while the lumbo-sacral spinal cord did not display any apparent change in proliferation (Yaghmaeian Salmani et al., 2018). To address proliferation in the hypothalamus, we used the CNS progenitor marker Sox2, phosphorylated Ser-28 on Histone 3 (PH3, a marker of mitotic cells), and 4',6-diamidino-2-phenylindole (DAPI) nuclear staining, to assess total nuclear (cellular) volume. Focusing on E15.5, in the *Eed-cKO* mutants we observed fewer PH3+ cells in the hypothalamus than in control ($Eed^{fl/fl}$) (Figure S2A-H). Quantification supported this notion and revealed significantly fewer PH3+ cells/DAPI volume and fewer PH3+ cells/Sox2 volume (Figure S2I-J). We did not however observe reduction of the percentage of Sox2 expressing cells/DAPI volume (Figure S2K). Hence, similar to our previous findings for the telencephalon (Yaghmaeian Salmani et al., 2018), *Eed-cKO* mutants displayed reduced proliferation in the hypothalamus during embryogenesis.

Single cell transcriptional profiling reveals upregulation of H3K36me3 marked genes in *Eed* mutants

To address the effects of *Eed* mutation upon hypothalamus development in more detail we performed scRNA-seq analysis. We focused first upon a late embryonic stage, E18.5, because

the majority of distinct neuronal sub-types – such as those specifically expressing neuropeptides and neurotransmitters – have been generated by this stage (Kim et al., 2020; Romanov et al., 2020; Zhang et al., 2021). We dissected the hypothalamus from 6 control (*Eed*$^{fl/fl}$) and 9 *Eed-cKO* embryos, at E18.5. Cells were dissociated and sequenced on the Illumina/Bio-Rad ddSEQ platform, yielding a total of 20,703 cells.

Based upon the distribution profile of unique molecular identifiers (UMIs) and UMIs/gene, we removed cells with fewer than 600 UMIs and less than 1.2 UMIs/expressed gene. The remaining 14,121 cells had a mean of 5,275 UMI counts/cell and 1.9 counts/expressed gene (Figure S3). Based on recent scRNA-seq analysis of the entire adult mouse nervous system (Zeisel et al., 2018) we identified non-neural cells e.g., vascular cells, blood cells and microglia, and because these would not have been targeted by *Sox1-Cre* (Yaghmaeian Salmani et al., 2018), we excluded them from further analysis. Moreover, *Foxg1* is expressed in the telencephalon and since its expression abuts the anterior extent of the hypothalamus (Figure 1A), these cells were also excluded. This yielded 11,713 hypothalamic neural cells, denoted "All-Hypo"; 6,202 cells from control and 5,511 cells from *Eed-cKO* embryos (Figure 1B). Uniform Manifold Approximation and Projection (UMAP) embedding, based upon the top-300 most variable genes (see Experimental Procedures; Table S1), illustrate this filtering process (Figure 1C).

To assess differential gene expression (DE) we used *DEsingle* (Miao et al., 2018). We categorized the effects as: differential abundance of cells expressing the gene (DEa), differential magnitude of gene expression (DEm), or general differential expression (DEg), which entails both differential abundance and magnitude. Analysing the All-Hypo cells revealed 5,421 DE genes, when comparing *Eed-cKO* to control (Table S2); 2,307 genes were upregulated and 3,114 were down-regulated. Of the upregulated genes, we found that 104 genes were DEa, 1 DEm, and 2,202 were DEg; while for the downregulated genes 11 were DEa, 0 DEm, and 3,103 DEg. Analysis for annotated gene sets enriched in our groupings of DE genes revealed an enrichment for genes involved in transcriptional regulation and H3K27me3 marked genes across the *ENCyclopaedia of DNA Elements* (*ENCODE*) (Davis et al., 2018). In addition, the upregulated DEg group also showed enrichment for H3K4me3 and H3K36me3 marked genes (Figure S4, Tables S3 and S4).

Single cell transcriptional profiling reveals cell cycle inhibitor upregulation and brain posteriorization in *Eed* mutants

Our previous study of *Eed-cKO* mutants revealed reduced proliferation in the developing telencephalon, accompanied by upregulation of two members of the Cip/Kip family of cell cycle inhibitors; *Cdkn1a* and *Cdkn1c* (Yaghmaeian Salmani et al., 2018). In line with these findings, analysing the All-Hypo cells, using UMAP embedding and DE analysis, revealed upregulation of *Cdkn1b* and *Cdkn1c* (both DEg), as well as of three of the four members of the INK4 family of cell cycle inhibitors, *Cdkn2a* (DEa), *Cdkn2b* (DEg) and *Cdkn2c* (DEg) (Figure 1D, Table S2).

Turning to developmental regulatory genes, UMAP embedding and DE analysis revealed that 33 out of the 39 Hox homeotic genes were upregulated in the *Eed-cKO* mutants (3 DEg, 29

DEa) (Figure 1E-F, Table S2). This is in line with our previous analysis of the telencephalon, using bulk RNA-seq, which showed upregulation of all 39 Hox genes, to levels matching their expression in the spinal cord (Yaghmaeian Salmani et al., 2018). Moreover, we observed that many other posteriorly expressed TFs were also upregulated, including *Pax2*, which displayed upregulation in the UMAP embedding, in the DE analysis (DEg) and on immunostaining (Figure 1G, S5A-F, Table S2). Hence, the scRNA-seq and immunostaining analysis revealed that *Eed-cKO* mutants displayed posteriorization and a reduced proliferative gene expression profile in the developing hypothalamus.

Single cell transcriptional profiling identified all major hypothalamic cell types at E18.5

The ectopic expression of a number of posteriorly expressed TFs suggested that hypothalamic cell specification may be strongly affected in the *Eed-cKO* mutants. To address this issue, we first analysed the generation of broader hypothalamic cell types (Chen et al., 2017; Kim et al., 2020; Romanov et al., 2020; Romanov et al., 2017). UMAP embedding of All-Hypo cells revealed that the major cell types were generated in *Eed-cKO* mutants, including GABAergic neurons (*Slc32a1*), glutamatergic neurons (*Slc17a6*), oligodendrocytes (*Olig1*), astrocytes (*Gfap*), ependymal cell (*Foxj1*) or tanycytes (*Rax*) (Figure 2A-F). Nevertheless, DE analysis did reveal minor downregulation of *Slc32a1* (DEg) and *Slc17a6* (DEg), while *Olig1* (DEg), *Gfap* (DEg), *Rax* (DEa) and *Foxj1* (DEg) were upregulated (Table S2). Moreover, we observed an apparent increase in the overlap between glutamatergic and GABAergic markers (*Slc32a1* and *Slc17a6*) (Figure 2E-F). Specific identification of double-positive cells confirmed this observation, revealing a significant increase in double-positive cells (Figure 2G, Fisher's Exact Test p-value < 1e-3). This effect prompted us to scrutinize the TF expression changes in the *Eed-cKO*. We noted that the *Tfap2a* and *Tfap2b* genes, known determinants of cerebellar GABAergic interneuron cell fate (Zainolabidin et al., 2017), were among the genes ectopically expressed (Figure 1G). This was apparent both in the UMAP embedding and the DE analysis (both DEg) (Figure 1G, 3E-F, Table S2). Immunostaining confirmed this upregulation. Specifically, in control, Tfap2b is restricted to posterior regions of the E18.5 brain. In contrast, in *Eed-cKO*, Tfap2b expression was apparent throughout the entire brain, including the hypothalamus (Figure 3A-D).

Hence, while all major hypothalamic sub-types were generated in *Eed-cKO*, there were effects on the partition of GABAergic and glutamatergic cell fate, and ectopic expression of the *Tfap2a* and *Tfap2b* GABAergic determinants.

Single cell transcriptional profiling reveals limited effects on hypothalamic cell fate specification in *Eed* mutants

Next, we focused on the generation of more discrete neuronal subtypes. We analysed the All-Hypo cells for their expression of 29 neuropeptide (NP) genes (Table S1), the *Th* and *Ddc* dopamine markers (DA), and the *Hdc* histaminergic marker, and thereby identified 8,219 "NP-

DA" cells within the All-hypo cells; 4,275 from control and 3,944 from *Eed-cKO* embryos. We created UMAP embedding of the NP-DA cells using the aforementioned NP-DA genes, as well as 90 additional genes found to be most correlated with the expression of the NP-DA marker genes (Table S1). In control, clustering and UMAP visualisation based upon these marker genes identified 116 major cell clusters (Figure 4A, 4C). Several clusters displayed co-expression of neuropeptides i.e., *Agrp-Npy*, *Avp-Gal*, *Kiss1-Tac2* and *Npy-Sst*, which is in agreement with previous scRNA-seq expression analysis in the adult and/or embryonic hypothalamus (Chen et al., 2017; Romanov et al., 2020; Romanov et al., 2017; Zhang et al., 2021). Expression of *Th* and *Ddc* is broader than DA neurons (Bjorklund and Dunnett, 2007), and *Th-Ddc* co-expression is only detected in two smaller cell clusters, which also express *Slc6a3*, identifying them as *bona fide* DA neurons (Figure 4A, 4C). Two neuropeptide genes (*Galp*, *Prlh*) were not detected.

Turning to the *Eed-cKO* mutants, in spite of the reduced proliferation and the ectopic expression of a number of posterior TFs, the UMAP embedding revealed surprisingly limited effects upon NP-DA cell specification in the E18.5 hypothalamus, as evidenced by the generation of the majority of the 116 NP-DA sub-types (Figure 4B-C). Specification of NP-DA sub-types occurred in spite of the ectopic expression of Hox and other regulatory genes within the majority of cell clusters (Figure S6A-B). For example, in control, *Avp* expressing cells separated into four clusters, all of which co-expressed other neuropeptide genes. All four Avp cell clusters were present in the UMAP from *Eed-cKO* mutants, in spite of the ectopic expression of Hox genes and other TFs in these cells (Figure 4A-D, S6A-B, Table S2). The generation of Avp neurons in *Eed-cKO* was also supported by immunostaining (Figure S7A-H).

Single cell transcriptional profiling reveals loss of DA neurons in *Eed* mutants

While the scRNA-seq and immunostaining analysis revealed that most NP-DA cell sub-types were generated in *Eed-cKO*, we noted several specific effects. Interestingly, UMAP embedding revealed that one of the *Ddc-Th-Slc6a3* clusters was largely lost in *Eed-cKO* mutants, while the other was reduced in size (Figure 4A-B). In line with this finding, *Ddc*, *Th* and *Slc6a3* were all significantly downregulated in *Eed-cKO* mutants (DEg) (Figure 4D, Table S2, Figure 5A-C). Studies of hypothalamic DA cells have revealed the involvement of several TFs, including Rax, Dlx1, Otp, Sim1 and Arnt2 (Biran et al., 2015; Orquera et al., 2016; Yee et al., 2009). Because the *Ddc-Th-Slc6a3* cells are largely missing in *Eed-cKO*, we could not determine the expression of these genes in the DA cells. However, DE analysis of the All-Hypo cells revealed that *Dlx1* and *Arnt2* were both downregulated in All-Hypo cells (both DEg), while, surprisingly, *Rax* was upregulated in All-Hypo cells (DEg) (Table S2). *Otp* was neither detected in control nor *Eed-cKO* (Table S2).

Single cell transcriptional profiling reveals loss of Hcrt neurons in *Eed* mutants

Turning to neuropeptide cells, while UMAP embedding did not reveal obvious effects in *Eed-cKO* upon the majority of neuropeptide genes, DE analysis did reveal minor effects upon a

number of them, including upregulation of 8 genes and downregulation of 7 genes (Figures 4D, 5D-E, S8, S9, Table S2). In contrast, for *Tac2*, while UMAP analysis revealed a complete loss of one *Tac2*-only cluster, this was not confirmed in the DE analysis, probably due to *Tac2* being expressed in three other clusters, which appeared unaffected in the UMAP (Figures 4A-B, 4D, 5D). The upstream regulatory cues specifying the different Tac2 neuronal sub-types is not well understood, precluding any assessment of potential causes of the loss of one specific Tac2 cluster.

We also observed strong effects upon *Hcrt*, both with respect to a near complete loss of cells expressing *Hcrt* in the UMAP, and to the expression levels (DEg) (Figure 4A-D, 5E, 6G-H, Table S2). This observation was confirmed by immunostaining (Figure 6A-D). Previous studies have identified several TFs that are involved in Hcrt cell specification, including Dbx1, Ebf2 and Lhx9 (Dalal et al., 2013; De La Herran-Arita et al., 2011; Liu et al., 2015; Sokolowski et al., 2015). In control *Hcrt* cells, *Lhx9* is the only TF gene of these three that is DE in *Hcrt* cells, when compared to other NP-DA clusters (Table S5). Because the *Hcrt* cells are missing in *Eed-cKO*, we could not determine the expression of *Dbx1*, *Ebf2* or *Lhx9* in these cells in the mutant. However, DE analysis of All-Hypo cells revealed that both *Ebf2* and *Lhx9* were downregulated (both DEg) (Table S2).

scRNA-seq at earlier stages reveals reduction of Lhx9 expressing progenitor cells in *Eed* mutants

To better understand the origins of the phenotypes observed at E18.5 we conducted scRNA-seq analysis of control and *Eed-cKO* at earlier stages; E13.5, E15.5 and E18.5. We generated a total of 51,540 high-quality cells: 21,335 from control and 30,205 from *Eed-cKO* mutants. Following the same biological filtering process as for E18.5, we yielded a total of 41,646 hypothalamic neural cells (All-Hypo); 18,551 cells from control and 23,095 cells from *Eed-cKO* embryos (Figure S10A-C). Additional stages from control were also generated to capture the transcriptional range of phenotypes across hypothalamic development for determining the UMAP embedding, though only equivalent stages were analysed for all subsequent statistical analysis (see Methods).

First, we focused first on the three NP-DA cell types affected at E18.5: the DA (*Slc6a3*), *Hcrt* and *Tac2* sub-cluster of cells. In control, all three cell types were evident also at the earlier embryonic stages. However, in *Eed-cKO* mutants there was a near complete loss of *Slc6a3* expressing cells, a complete loss of high-expressing Hcrt cells, and loss of one *Tac2* cluster across all stages (Figures 7E, S10C). Hence, all three NP-DA cell types that were affected at E18.5 were also affected at earlier stages.

To address broader aspects of development we utilised a binary labelling method with cell type marker genes (see Methods), according to broad cell types such as Glutamatergic, GABAergic, sub-ventricular zone, ventricular zone, and various glial cell types (Figure S10C). We noticed two major differences between control and *Eed-cKO*. First, the loss/reduction of a particular subpopulation of progenitor cells (Hes5-, Sox2+) (Figures 7F, S10C). Because Lhx9 is

one of the few known transcription factors involved in *Hcrt* cell specification and was significantly downregulated in *Eed-cKO* at E18.5, we examined *Lhx9* expression in the temporal UMAP space. This revealed that the specific Hes5-, Sox2+ progenitor population that displayed loss/reduction in *Eed-cKO* also co-expressed *Lhx9* (Figure 7F-H). Gene expression analysis of the *Lhx9* group of cells between control and *Eed-cKO*, as well as against all mutant cells (Table S9, S10) revealed significant upregulation of many developmental regulators in the *Lhx9* population, including 29/39 of the Hox transcription factors (Figure 7I, Table S11). Second, similar to what was observed at E18.5 we noted significantly higher numbers of Glut/GABA cells in *Eed-cKO* mutants (Figure 7A-D, Fishers exact test, $p<1e-3$). Again, gene expression analysis revealed ectopic expression of developmentally important genes in the Glut/GABA cells, such as *Tfap2a/b* and *Pax2* (Figure 7C,I, Table S11). We observed significantly greater ectopic expression of developmental regulators in both the *Lhx9* and Glut/GABA cells, when compared to all other cells (Figure 7I, Table S11), revealing that these two cell populations were particularly affected.

In summary, *Eed-cKO* mutants display a loss of the H3K27me3 mark from E11.5 and onward, posteriorization of the hypothalamus, and reduced proliferation. Despite these effects most major neuronal sub-types are generated by E18.5. However, there is an increase in the number of Glut/GABA co-expressing cells, and loss/reduction of DA, *Hcrt* and a sub-set of *Tac2* neurons. These effects are likely due to the up- and downregulation of several known upstream regulators in specific subpopulations of progenitors. Interestingly, despite the gradual loss of H3K27me3, we did not observe any apparent correlation between the specific cells affected and the onset of their marker genes (Table S6).

DISCUSSION

Gradual loss of H3K27me3 in *Eed* mutants

Epigenomic methylation marks are generally viewed as stable over time. However, they are subjected to two main removal cues: de-methylation and replication-mediated dilution. How do these removal dynamics fit with the observed gradual reduction of H3K27me3 in *Eed-cKO*?

De-methylation of H3K27me3 is chiefly mediated by *Kdm6a* (*Utx*) and *Kdm6b* (*JMJD3*) (Arcipowski et al., 2016). However, while mutation of *Kdm6a* and/or *Kdm6b*, in mouse or ESCs, did result in elevated H3K27me3 levels at specific loci, there was no global increase in H3K27me3 levels (Burgold et al., 2008; Park et al., 2014; Tang et al., 2020; Wijayatunge et al., 2018). Similarly, in *Drosophila*, *Utx* mutation did not alter the dynamics of H3K27me3 reduction at a specific target locus in the developing wing disc (Laprell et al., 2017). Hence, while de-methylation mediated by Kdm6a/b modulates H3K27me3 levels, it does not appear to play an instrumental role in counteracting PRC2 activity at all target loci.

By contrast, DNA replication can efficiently reduce the levels of the H3K27me3 mark by H3 dilution, as new nucleosomes form post replication. Studies in *Drosophila* have found that removal of a Polycomb Response Element (PRE) at a target locus resulted in the gradual reduction of H3K27me3, with some 50% reduction per cell cycle, and loss of transcriptional repression already after one cell cycle (Coleman and Struhl, 2017; Laprell et al., 2017). Similarly, studies of the mouse intestine have revealed that loss of PRC2 activity (by *Eed* or *Ezh2* mutation) resulted in the gradual loss of H3K27me3 levels, also with an estimated 50% reduction per cell cycle (Jadhav et al., 2020).

To circumvent early embryonic lethality we inactivated *Eed* using the early neuroectodermal Cre deleter, *Sox1-Cre*, (active at E8.5) (Takashima et al., 2007). This resulted in a gradual loss of the H3K27me3 mark in the *Eed-cKO* mutants, with reduction in immunostaining at E10.5 and complete loss at E11.5, in the telencephalon, spinal cord and hypothalamus (Yaghmaeian Salmani et al., 2018) (herein). We envision that some of the delay in H3K27me3 reduction results from the delay in deletion of both gene copies, as well as the degradation of wild type *Eed* mRNA and Eed protein, the latter of which may be especially slow for Eed protein that is associated with the PRC2 complex. In addition, a major part of the gradual reduction of H3K27me3 levels is likely connected to proliferation dynamics. Progenitor cycling speeds have not been mapped in the early mouse hypothalamus, but studies of the E11 mouse telencephalon has revealed neuroepithelial progenitor cell cycle speeds of 8-10 hrs (Caviness et al., 1995; Takahashi et al., 1995). In light of these studies, the gradual loss of the H3K27me3 mark in *Eed-cKO* mutants, being reduced at E10.5 and lost at E11.5 i.e., 2-3 days and hence some 6-9 cell divisions after *Eed* inactivation at E8.5, is consistent with a replication-mediated dilution of modified H3 histones.

Reduced proliferation in *Eed-cKO* mutants

Previous studies of *Eed-cKO* mutants revealed reduced proliferation in the telencephalon (Telley et al., 2019; Yaghmaeian Salmani et al., 2018), which was accompanied by increased expression

of the Cip/Kip cell cycle inhibitors *Cdkn1a* and *Cdkn1c* (Yaghmaeian Salmani et al., 2018). Here, we observed reduced proliferation also in the hypothalamus, and upregulation of *Cdkn1b* and *Cdkn1c*, as well as *Cdkn2a*, *Cdkn2b*, and *Cdkn2c*, in the E18.5 scRNA-seq data. It is likely that the upregulation of most of the Cip/Kip and INK4 cell cycle inhibitor genes is a major reason for the reduced proliferation in *Eed-cKO* mutants.

The reduced proliferation in the hypothalamus begs the question of which cells are not being generated. Recent scRNA-seq analysis of the developing hypothalamus has revealed that neurons are generally born earlier than other cell types, appearing already at E10 and onward, and that glia, ependymal cells and tanycytes appear from E16 and onward (Kim et al., 2020; Romanov et al., 2020; Zhang et al., 2021). Our UMAP embedding of the All-Hypo cells did not reveal striking loss of any major cell type i.e., GABAergic neurons, glutamatergic neurons, astrocytes, oligodendrocytes, ependymal cells and tanycytes. However, we observed an increase in Glu/GABA co-expressing cells. Single expressing Glu and GABA cells, as well as Glu/GABA co-expressing cells, are born early during hypothalamic development, but are also added throughout embryogenesis [herein (Kim et al., 2020; Romanov et al., 2020; Zhang et al., 2021)]. Against this backdrop, it is not apparent if/how the reduced proliferation observed in *Eed-cKO* mutants could act to increase the number of Glu/GABA co-expressing cells.

Regarding NP-DA subtypes, while the actual birth-date for most hypothalamic neuronal subtypes has not been determined, the onset of NP-DA marker expression has been analysed in most cases (Table S6). Assuming a gradual loss of the H3K27me3 mark, a logical effect would be the loss of late-expressing NP-DA markers, indicating a failure to generate late-born neurons. However, the subtypes affected do not apparently link to marker gene expression onset, with genes activated both early (E11.5) and late (E15.5) being affected, or alternatively, unaffected (Table S6). Hence, the differential effects upon discrete cell subtypes are not readily explained by differential birth dates.

Previous analysis in the telencephalon revealed that *Eed-cKO* mutation primarily affected the proliferation of daughter cells, as opposed to progenitor cells (Yaghmaeian Salmani et al., 2018). Recent studies, including genetic lineage tracing, have revealed a complex repertoire of progenitor and proliferative daughter cells in both the mouse and human hypothalamus, which in many aspects are similar to the developing telencephalon (Zhang et al., 2021; Zhou et al., 2020). It is tempting to speculate that the selective effects of *Eed-cKO* upon cellular subtypes born both early and late may relate to the lineage topology of different hypothalamic lineages, an issue of which we still know very little.

Eed-cKO triggers posteriorization of the brain

A well-conserved role of PRC2 in Bilaterians is to confine Hox homeotic gene expression to the posterior CNS (Isono et al., 2005; Li et al., 2011; Struhl, 1983; Struhl and Akam, 1985; Suzuki et al., 2002; Wang et al., 2002; Yaghmaeian Salmani et al., 2018). Our previous studies of *Eed-cKO* mutants confirmed this role for PRC2, and we observed ectopic expression of all 39 Hox homeotic genes in the E15.5 mouse forebrain, as revealed by bulk RNA-seq (Yaghmaeian

Salmani et al., 2018). We also observed several other, posteriorly expressed TFs being ectopically expressed in the forebrain. Here, using scRNA-seq, we find similar effects in the developing hypothalamus. A growing body of work is pointing to the role of Hox genes in regulating cell cycle genes and repressing proliferation (Economides et al., 2003; Monedero Cobeta et al., 2017; Yaghmaeian Salmani et al., 2018). Strikingly, in *Drosophila*, simultaneous removal of Hox genes can rescue reduced proliferation in *esc* mutants (the *Drosophila* orthologue of *Eed*) (Bahrampour et al., 2019). These studies indicate that the reduced hypothalamic proliferation observed in *Eed-cKO* may be a direct result of the posteriorization of the entire fore- and midbrain, and the ectopic expression of posterior Hox homeotic genes.

Enrichment of H3K36me3 in genes repressed by PRC2

The recruitment of PRC2 to chromatin and the control of its local activity has been, and continues to be, under intense investigation. This issue is further complicated by the finding that different PRC2 sub-complexes have different properties. There are five major recruitment and/or activity interaction nodes for mammalian PRC2: low-methylated CpG islands, H2AK119ub, H3K27me3, H3K36me3 and RNA (Chammas et al., 2020; Laugesen et al., 2019; Mocavini and Di Croce, 2020; van Mierlo et al., 2019). Recent studies found that activation of genes repressed by PRC2, post *Eed* or *Ezh2* mutation, was positively correlated with the levels of not only H3K27me3, but also the H3K4me3 active mark (Jadhav et al., 2020). In line with these findings, our GO enrichment analysis also identified an enrichment of DE genes marked by H3K27me3 and H3K4me3. In addition, we observed enrichment of the H3K36me3 mark, specifically in the upregulated genes. While generally regarded as an activating mark, acting by repressing PRC2 docking and activity (Finogenova et al., 2020), H3K36me3 has also been proposed to selectively mark genes for future H3K27me3 modification and subsequent repression to facilitate transition from pluripotency to post-mitotic cell fates [reviewed in (Abed and Jones, 2012)]. Since the category “upregulated DEg genes” represent those that had both increased magnitude of expression and an increased number of cells expressing that gene, it is possible that this group of genes may represent those that should have been repressed by PRC2 to facilitate transition to post-mitotic cell fates.

Selective involvement of *Eed* upon hypothalamic cell fates

In *Eed-cKO* mutants, despite the reduced proliferation and upregulation of many posteriorly expressed developmental regulators, we observed that the majority of neural sub-types were still generated. One possible explanation for the limited effects observed may be that *Eed-cKO* results in the loss of H3K27me3 subsequent to that many important developmental decisions, i.e., patterning of the hypothalamic progenitor region, have already played out, during E8-E11 (Alvarez-Bolado, 2019; Bedont et al., 2015; Blackshaw et al., 2010; Burbridge et al., 2016; Ferran et al., 2015; Puelles and Rubenstein, 2015; Xie and Dorsky, 2017). Nevertheless, major aspects of neurogenesis and cell specification do occur subsequent to E11.5, and while there is

extensive mis-regulation of a large number of genes it is surprising that H3K27me3 is apparently not critical for many of the genetic cascades that govern cell fate.

Although many cell types are present, we did observe an increase in Glut/GABA co-expressing cells, apparent at all stages analysed. We observed DE of a number of TFs, including ectopic expression of the cerebellar GABA determinants *Tfap2a* and *-b* (Zainolabidin et al., 2017), and their expression showed extensive overlap with Glut/GABA co-expressing cells.

In addition, *Eed-cKO* mutants also displayed the absence of DA and Hcrt cells, as well as a subset of Tac2 cells. While the absence of these cells in *Eed-cKO* mutants hindered detailed analysis of the underpinnings of these phenotypes, we observed that two of the three known regulators of hypothalamic DA cells, *Dlx1* and *Arnt2*, were downregulated. Similarly, we observed down-regulation of two of the three known regulators of *Hcrt* cells, *Ebf2* and *Lhx9*. Down-regulation of these TF genes may indeed explain the absence of DA and Hcrt cells. Indeed, analysis of earlier stages revealed that a subset of *Lhx9* positive progenitors (Sox2+) are missing in the mutant. Specification of the different *Tac2* neuronal sub-types has not been previously addressed, and hence the underpinnings of this phenotype is currently unclear.

Are there any commonalities between DA, Hcrt and Tac2 neurons that could explain the absence of these three particular cell types? The specific progenitor region of origin for the different hypothalamic DA neuron sub-types (A11, A12, A14, A15), Hcrt or Tac2 neurons is not clear, but their final cell body locations (DA neurons medial, Hcrt neurons lateral and Tac2 neurons in several regions) argue against a common origin. Similarly, the non-overlapping sets of upstream regulators, Otp, Sim1 and Arnt2 for DA neurons (Biran et al., 2015), and Dbx1, Ebf2 and Lhx9 for Hcrt neurons (Dalal et al., 2013; De La Herran-Arita et al., 2011; Liu et al., 2015; Sokolowski et al., 2015), also argue against a common origin, as well as against a common genetic pathway. Interestingly, knock-out of the H3K4-methyltransferase *Mll4* gene in the developing hypothalamic arcuate nucleus also resulted in highly selective effects on neuronal sub-type specification (Huisman et al., 2021).

Implications for PRC2 sensitivity

A growing body of work points to the role of epigenetics in gating entry into puberty, in particular with respect to controlling the expression of neuropeptide genes involved in triggering puberty, such as *Kiss1* and *Tac2* (aka *Tac3*) (Aylwin et al., 2019; Shalev and Melamed, 2020). This pertains specifically to the PRC2 complex, which plays a major role in gating the elevated expression of the *Kiss1* and *Tac2* genes necessary for puberty. Analysis of a number of PRC2 genes revealed that *Eed* gene expression is downregulated in the hypothalamus pre-puberty, followed by *Kiss1* and *Tac2* upregulation. Strikingly, overexpression of *Eed* resulted in repression of *Kiss1* gene expression and an inhibition/delay of puberty (Lomniczi et al., 2013). We did not, however, observe any upregulation of *Kiss1* or *Tac2* in our *Eed-cKO* scRNA-seq data (Table S2), but rather the loss of a distinct cluster of *Tac2* expressing cells. These findings indicate that the epigenomic profile of the *Kiss1* and Tac2 promoters and their sensitivity to

PRC2 may change from embryogenesis to early adult life, and from "baseline" to elevated levels of expression.

Finally, in humans, extensive genome and exome sequencing points to that all major PRC2 components, including *EED*, are haploinsufficient (Karczewski et al., 2020). In line with this, a group of related human developmental overgrowth syndromes, including the Weaver, Weaver-like, Cohen-Gibson, and Overgrowth and Intellectual Disability syndromes, appears to be caused by heterozygous mutations in *EED*, *EZH2* or *SUZ12* (Burkardt et al., 2019; Cyrus et al., 2019). These syndromes manifest with peripheral overgrowth, as well as neurological defects and intellectual disability. Our finding of a particular sensitivity of DA, Hcrt and Tac2 neurons to loss of PRC2 activity may suggest that behaviours related to these hypothalamic cell types may be important to assess in the human PRC2 syndromes. This applies particularly to the effect of PRC2 on the hypothalamic DA neurons, which are known to repress Growth Hormone release from the pituitary (De Zegher et al., 1993; Van den Berghe et al., 1994a; Van den Berghe et al., 1994b), hence forming a plausible link between DA neuron loss and general overgrowth in the PRC2 syndromes.

ACKNOWLEDGEMENTS

We are grateful to Jose Dias, Johan Ericson, The Jackson Laboratory mouse stock centre and the ENCODE consortium, for sharing reagents and advice. We thank Nigel Kee and Brian Key for critically reading the manuscript. Carolin Jonsson provided excellent technical assistance.

COMPETING INTERESTS

No competing interests declared.

FUNDING

Funding was provided by the Swedish Research Council (621-2013-5258), the Knut and Alice Wallenberg Foundation (KAW2011.0165; KAW2012.0101), the Swedish Cancer Foundation (140780; 150663), and the University of Queensland, to ST, by an Australian Government RTP Scholarship to BB, by an Australian Research Council Discovery Project grant (Australian Research Council (DP180100017), to MP, and by Swedish Research Council (2016-02506) and Torsten Söderberg Foundation, to TP.

MATERIALS AND METHODS

Mouse stocks

The *Eed*$^{fl/fl}$ allele has exons 3-6 flanked by *loxP* sites (Xie et al., 2014), and was obtained from Jackson Laboratory Stock Center (Bar Harbor, Maine, USA; stock number #022727). The *Sox1-Cre* line (Takashima et al., 2007) was provided by Jose Dias and Johan Ericson (Karolinska Institute, Stockholm, Sweden). Stocks were maintained on a *B6:129S1* mixed background. Mice were maintained at Linkoping University animal facility, in accordance with best practices. All mouse procedures were approved by the regional animal ethics committee (Dnr 69-14). The morning of the vaginal plug was set as 0.5 days post coitum i.e., E0.5. Pregnant females were sacrificed, and embryos dissected at E12.5, E13.5, E15.5, E16.5 and E18.5. Primers for genotyping were: Cre1: GCG GTC TGG CAG TAA AAA CTA TC. Cre2: GTG AAA CAG CAT TGC TGT CAC TT. Eed1: GGG ACG TGC TGA CAT TTT CT. Eed2: CTT GGG TGG TTT GGC TAA GA. Male/female primers (Clapcote and Roder, 2005); forward: CTG AAG CTT TTG GCT TTG AG; reverse: CCA CTG CCA AAT TCT TTG G.

Immunohistochemistry

Mouse embryos were dissected to extricate the brains, which were fixed in 4% PFA at +4°C for 18-36h, and kept in 30% sucrose at 4°C until saturated, upon which they were frozen in OCT Tissue Tek (Sakura Finetek, Alphen aan den Rijn, Netherlands) and stored at -80°C. Cryosections (30 µm) were treated with 4% PFA for 15 min at room temperature, blocked and processed with primary antibodies in PBS with 0.2% Triton-X100 and 4% horse serum overnight at +4°C. Secondary antibodies, conjugated with AMCA, FITC, Rhodamine-RedX, Cy5 (Jackson ImmunoResearch, West Grove, PA, USA), or AFD555, AF568 or AF647 (Thermo Fisher Scientific, Waltham, MA, USA), were used at 1:200. Slides were mounted in Vectashield (Vector Laboratories, Burlingame, CA, USA). DAPI was included in the secondary antibody solution. Primary antibodies: Goat anti-Sox2 (1:250, #SC-17320, Santa Cruz Biotechnology, Santa Cruz, CA, USA). Rabbit anti-H3K27me3 (1:500, #9733, Cell Signaling Technology, Leiden, Netherlands). Rat anti-PH3-Ser28 (1:1,000; Cat.no. ab10543). Rabbit anti-Pax2 (1:100, #ab232460), rabbit anti-TFAP2b (1:100, #ab221094), rabbit anti-Orexin A (Hcrt) (1:1,000, ab6214), rabbit anti-Avp (1:500, #ab213708, Abcam, Cambridge, UK).

Confocal Imaging and Data Acquisition

Fluorescent images were obtained with Zeiss LSM700 or Zeiss LSM800 confocal microscopes. Confocal stacks were merged using Fiji software (Schindelin et al., 2012). Compilation of images and graphs was done in Adobe Illustrator.

Quantification of proliferation

On confocal images of sagittal sections, a selection was made along the rim of the hypothalamic tissue, of 400 µm width (segmented line), using ImageJ (Fiji) software. This selection was straightened. A second sub-selection of 1000 µm in length of the straightened tissue was made. The final tissue selection analysed was 400 x 1000 µm.

PH3, DAPI and Sox2 staining were quantified using Fiji software (Schindelin et al., 2012; Schindelin et al., 2015). 3D reconstruction and volume quantification of DAPI and Sox2 signals were achieved using 3DViewer Fiji plugin (Schmid et al., 2010) in the selected regions and considering the anatomical features, excluding non-CNS tissue. Mitotic cells (PH3+) were counted in the selected region (mentioned above). Proliferation analyses are presented as ratios of mitotic cells to DAPI or Sox2 calculated volumes within the selected regions. ImageJ (Fiji) thresholding methods (functions) “Huang” & “Moments” were used to remove background/noise from signal in volumetrics analysis of Sox2 and DAPI, respectively.

Mitotic analysis

For mitotic analyses, two-tailed Student´s T-test was performed. One (*), two (**) or three (***) asterisks were used to assign statistical significance of $p \leq 0.05$, $p \leq 0.01$ or $p \leq 0.001$ respectively. Microsoft Excel 2010 and GraphPad Prism 8.3.0 were used for statistical analyses, data compilation and graphical representation.

scRNA-Seq

Data generation

E12.5, E13.5, E15.5, E16.5, & E18.5 embryos (control: E12.5, E13.5, E15.5, E16.5 and E18.5; *Eed-cKO*: E13.5, E15.5 and E18.5) embryos were harvested and genotyped. The hypothalamus was dissected out in ice-cold RPMI-1640 medium (cat.no. 11530586, Thermo Fisher Scientific, Waltham, MA, USA). The dissected hypothalamuses were further divided into 2-4 pieces before cell dissociation for single cell isolation using Papain Dissociation System (cat no. LK003150, Worthington Biochemical Corporation, Lakewood, NJ, USA). The tissues were incubated with papain solution at +37°C for 60 min, under slow shaking (80 rpm). Isolated single cells were re-suspended in ice-cold 1xPBS, 0.1% BSA, to a final concentration of 2,500 cells/µl (+/- 10%). Cells were checked for viability using a Bio-Rad TC10 automated cell counter (Bio-Rad, Hercules, CA, USA). Single cells and barcode beads were encapsulated into droplets using Bio-Rad ddSEQ Single-Cell Isolator for cell lysis and barcoding (cat.no. 12004336, Bio-Rad, Hercules, CA, USA). Subsequently, RNA-seq libraries were generated using Illumina SureCell WTA 3' Library Prep Kit for the ddSEQ System (6 cartridge version, cat.no. 20014280, Illumina, San Diego, CA, USA). Libraries were assessed for quality, using 1µl of undiluted cDNA, on an Agilent Technology 2100 Bioanalyzer, using an Agilent High Sensitivity DNA chip (cat.no. 5067-4626, Agilent, Santa Clara, CA, USA) to determine fragment size and yield. Samples were stored at -20°C until sequencing. Libraries were normalized and sequenced in pools of four, whereby libraries prepared on the same ddSEQ cartridge were balanced between different library pools to control for batch effects. The libraries were sequenced on an Illumina NextSeq500

system, using NextSeq 500/550 High Output Kit v2.5 (150 Cycles, cat.no. 20024907, Illumina, San Diego, CA, USA), paired-end read type and Single-Index. This platform does not have physically separate sequencing lanes, and thus pooled samples were sequenced over all four lanes of the NextSeq flow cell. The scRNA-seq fastq files were generated using the Illumina Base Space application *FASTQ Generation* v1.0.0.

Cell count matrix generation and quality control

Cell Unique Molecular Identifier (UMI) counts were generate using the Illumina Base Space application *SureCell RNA Single-Cell* v1.2.0; which uses using *STAR* (v2.5.2b) to align the cDNA reads to the mm10 genome (the second read mate, R2) and *samtools* (v1.3) to append cell barcodes to aligned reads (derived from the first read mate, R1). The generated counts for each sequencing run in each sample were concatenated into a single count matrix; yielding a total of 20,703 cells. For technical quality control, cells with fewer than 600 UMIs, less than 1.2 UMIs/expressed gene, and less than 300 genes expressed were removed. This resulted in 14,121 high quality cells (All-Cells). These had median values of 4,559 UMIs per cell, 2,430 expressed genes per cell, and 1.87 UMIs/gene expressed (Figure S3).

We then performed biological filtering in order to remove cells which do not develop within the hypothalamus. For these steps, we used ~500,000 reference single cell expression profiles with cell type labels (TaxonomyRank4 labels) from the mouse nervous system (http://mousebrain.org/downloads.html) (Zeisel et al., 2015), in combination with *scmapCluster* from *scmap* v1.4.1, to obtain initial cell type labels. Cells that do not develop within the hypothalamus were filtered, which included vasculature and immuno-related cell types (Vascular Endothelial, Vascular/Leptomeningial, Pericytes, Microglia).

Cells expressing *Foxg1* were also removed, since *Foxg1* expression demarcates the anterior extent of the hypothalamus (Figure 1). This resulted in 11,713 hypothalamic cells (All-Hypo). Cells were then normalized according to counts per ten-thousand (CPT) and log transformed (log2((gene-UMIs/cell-UMIs)*10 000)+1, i.e. log2(CPT+1)). The same biological filtering and quality control procedure was also applied to cells generated at the earlier embryonic time points (Figure S10).

Dimensionality Reduction

The main goal of our dimensionality reduction procedure was to capture a joint space of the control and Eed-cKO cells that would allow direct comparison of cellular diversity. Toward this end, we utilised *Principal Components Analysis* (*PCA*) for initial dimensionality reduction. PCA requires the input data to be mean-centred and variance-normalised per gene. In order to satisfy these requirements, we mean-centred and scaled to unit variance our normalised gene expression matrix using the *scale* function is *scikit-learn v0.21.3* prior to any PCA transformation. Importantly, we then derived the PCA transformation on the control cells alone, and then applied the same transformation on the *Eed-cKO* cells. This ensured that our dimensionality reduction captured the main dimensions of variation in the control cells and not sources of variation due to

the *Eed-cKO* treatment; hence allowing a direct comparison between these two conditions without complicated batch correction techniques. The PCA spaces of the two sets of cells were then concatenated, and *Uniform Manifold Approximation and Projection* (*UMAP*) was performed on this joint space using *umap-learn* v0.3.8. The genes used for each PCA prior to UMAP embedding are provided in Table S1; these were selected depending on the set of cells analysed, as detailed below.

Gene Selection

To prioritise the biological variation, we were interested in – primarily neurotransmitter, neuropeptidergic and DArgic diversity – we curated lists of marker genes for such populations. To counteract technical noise from utilising few genes we selected additional genes based on their correlation with these marker genes (as detailed for the specific analyses below). This approach was inspired by the method Garnett, which performs similar analyses for cell type prediction (Pliner et al., 2019). As evidenced by our resulting clustering and UMAP embeddings, this approach successfully allowed us to analyse hypothalamic cellular diversity in our control and *Eed-cKO* mice.

E18.5 All-Hypo Cells Analysis

To investigate the effect of *Eed-cKO* on broad hypothalamic cell types, we compiled a list of marker genes for neurons (GABAergic, glutamatergic) and glia (oligodendrocytes, astrocytes, tanycytes, ependymal cells). These are provided in Table S1. We subsequently labelled cells according to their type based on which marker gene they expressed the most highly. Cells not found to express any of these marker genes but expressing NP-DA markers were labelled as 'other-neuron'. Cells not expressing any differentiated cell type marker were considered un-labelled.

We then selected additional genes which would maximally separate our cell type labels using *normalised mutual information* (NMI, *scikit-learn* v0.21.3), a measure of correlation between discretely labelled data. To obtain discrete labels for gene expression, we classified genes as ‘on’ (counts>0), or ‘off’ (counts=0). We then selected the top 300 genes with the highest NMI (see Table S1) between the binary expression of that gene and the cell type labels. Using these marker genes, the dimensionality reduction procedure was performed as detailed above; with the top 100 principal components using 50 nearest neighbours, a minimum distance of 0.3, and the correlation distance metric as input to UMAP.

E18.5 NP-DA Cells Analysis

Cells were considered NP-DA if they expressed any of 32 neuropeptidergic or DA-ergic marker genes compiled from the literature (Table S1). 8,219 hypothalamic NP-DA cells were isolated from the rest of the cells prior to application of dimensionality reduction (detailed above) based on the 32 marker genes, along with the top 90 genes that had the highest Pearson correlation coefficient for at least one of the marker genes. The UMAP was performed based on the top 60

principal components using 10 nearest neighbours, a minimum distance of 0.01, a spread of 10, and the Manhattan distance metric.

E18.5 NP-DA Cell Clustering and Differential Gene Expression

Within the UMAP space containing both the control and *Eed-cKO* NP-DA cells, a nearest neighbour graph was constructed using the kneighbours_graph function in sklearn, with 4 neighbours and the Euclidean distance measure. The cells were subsequently clustered using the Lieden algorithm (*liedenalg v0.8.2*) with a resolution of 2. This resulted in 149 clusters. To derive the meaning behind the clustering, we used differential gene expression to label clusters according to the combination of NP-DA markers they upregulated. Significantly differentially expressed genes were determined for each cluster using independent t-tests *(scipy v1.4.1*), with a one-versus-rest mode of comparison (Bonferroni p-value < 0.05). We found this method of calling differential expression yielded the most reasonable number of differentially upregulated genes in order to distinguish each cluster, as opposed to Student's t-test which yielded many clusters with no NP-DA markers DE, and Wilcoxon rank-sum tests which yielded many clusters with numerous NP-DA markers DE (data not shown).

In cases where no NP-DA marker was found to particularly distinguish that cluster, clusters were labelled with the NP-DA markers with the highest proportion of expression in that cluster along with the best distinguishing gene in the extended list of genes used to derive the NP-DA UMAP (Table S1). Clusters were subsequently merged if they were found to upregulate the same combination of NP-DA marker genes and were neighbours in the UMAP space, or the cluster was not found to upregulate any marker but was spatially close in the UMAP space to another cluster and showed clear visual expression of the same marker gene.

This manual curation resulted in 116 hypothalamic NP-DA clusters. The aforementioned method for calling differentially expressed genes was subsequently re-run to ensure the markers remained DE in the final clusters; and to call differentially expressed genes within clusters between *Eed-cKO* and control cells (Table S5).

The heatmaps were constructed by taking the average expression of each gene in each NP-DA cluster segmented by control and *Eed-cKO*. The average expression of each gene across the NP-DA clusters was scaled between 0 and 1, to thereby visualise the expression in each cluster relative to the total across the clusters. Scaling was performed to enable direct comparison between the control and *Eed-cKO* heatmaps. These visualisations were constructed using *seaborn* v0.11.0.

E18.5 Broad Differential Expression and Gene Set Enrichment

Differential expression of control versus *Eed-cKO cells* - regardless of cluster - was performed using DEsingle (Miao et al., 2018). This resolved genes into different types of differential expression; differential abundance of cells expressing the gene (DEa); differential magnitude of gene expression (DEm); or general differential expression (DEg), where there is a change in both the abundance of cells expressing the gene and the magnitude with which that gene is expressed.

This differential expression was performed for the All-Hypo cells and the NP-DA cells separately (Table S2).

To investigate if the grouping of the genes into the types of differential expression had a biological significance, we performed gene set enrichment using the *Enrichr* method, grouping the genes into up- or down- regulated genes for each of the DEa, DEm, and DEg genes using gseapy v0.9.16 (Figure S4). We tested for enrichment using the *GO_Molecular_Function_2018* and the *ENCODE_Histone_Modifications_2015* gene sets, thus giving us insight into the molecular function and the epigenetic modifications of these genes across tissues (adjusted $p \leq 0.5$; Tables S3 and S4).

When visualising these results, we grouped terms based on similarity (Figure S4). Terms were grouped as "TF activity/DNA binding" if they mentioned "binding" or "transcription". Terms were grouped as "H3K27me3", "H3K36me3" or "H3K4me3" if either of these epigenetic marks were mentioned in the term name; all remaining terms were grouped as 'Other'. These groupings were based on a manual inspection of the enriched terms which revealed an over-representation of terms related to the aforementioned groupings.

Violin plot visualisations of the DE genes only included 5% of zeros for each grouping of cells, to prevent most of the density falling at zero. In the construction of the 'Transcription Factor' violin plot in Figures 1 and S6, we display the top upregulated genes in the *Eed-cKO* that appear in the GO term *DNA-binding transcription factor activity* (GO:0003700). The violin plots were constructed using *seaborn* v0.11.0.

Early Timepoint Cell Labelling

After quality control, as previously described, we subsequently labelled cells (control: E12.5, E13.5, E15.5, E16.5, & E18.5; *Eed-cKO*: E13.5, E15.5, E18.5) based on expression of known marker genes for glutamatergic, GABAergic, glial, and ventricular zone and subventricular zone cell types; the full cell type and marker list can be seen in Table S8. Due to varying specificity of markers for their respective cell types, we marked cells as belonging to a particular group in a hierarchical manner to alleviate this problem; whereby least specific markers were used to mark cells first, and most specific markers to mark cells last such that prior labelling's was overridden. The order this was performed is also shown in Table S8, where groups labelled first to last are listed from the top row of the table to the bottom row of the table.

A gene was considered 'on' in a particular cell if that cell expressed the gene in the upper 40^{th} percentile of the non-zero gene expression range of that gene. Labelling of cells was performed based on this binarization ('on'/'off') transformation of the gene expression in each cell. In the labelling process, we also considered negative gene expression indicators for particular cell types, and also 'or' and 'and' logic, where cells could be considered of a certain type if they expressed/did not express indicated marker genes in part or in combination. The exact logical notation used in each case is provided in Table S8.

As a further contingency to prevent labelling cells incorrectly and to reduce the number of unlabelled cells, we then trained a logistic regression classifier (as implemented in sklearn v0.22.2)

using all the genes present in Table S8 as well as all mouse transcription factors (as listed in GO term GO:0003700). To train the classifier on relevant genes with this set, we selected the top 300 genes which when considering their binarized expression (expression > 0) that had the highest normalised mutual information score with a randomly selected 80% of cells labelled using marker genes as a training set. We then trained the logistic regression classifier on this training set using the L1 penalty and liblinear solver, and then predicted the labels for the remaining 20% of binary labelled cells and the unlabelled cells. If the probability of the most likely predicted label for a given cell was smaller than 0.5, the cell was labelled 'unknown'. The confusion matrix for the left out 20% of cells are presented in Table S8, showing the labelling approach taken was effective in labelling the numerous kinds of broad cell types.

Early Timepoint Dimensionality Reduction

We performed dimensionality reduction as described above; except the gene set used was the top 300 most highly informative genes used for training the logistic regression classifier for the early timepoint cell labelling. The UMAP was then performed by creating a nearest-neighbours graph using scanpy v1.6.1 with 10 neighbours and the top 40 principal components, followed by scanpy's UMAP function applied with default settings. Notably, for the control cells we sampled a much greater range of time points (E12.5, E13.5, E15.5, E16.5, & E18.5) than *Eed-cKO* (E13.5, E15.5, and E18.5) in order to create a joint space more reflective of the developing hypothalamus. For all subsequent analyses comparing control with *Eed-cKO*, we compare only the overlapping time points (E13.5, 15.5, and E18.5) to prevent biological confounding from the additional time points in the control condition.

Early Timepoint Identification of *Eed-cKO* Affected Genes in Lhx9 and Glut/GABA cells

We first called differentially expressed genes between control & *Eed-cKO* within the groups of Lhx9 and Glut/GABA cells using a pseudosampling approach followed by a t-test to call DE genes. Namely, we created 20 random samples of approximately equal numbers of cells without replacement within each group/condition combination. The gene expression of these pseudosampled groups were then averaged, and DE genes were called between between *Eed-cKO* and control using a t-test (scanpy) with each pseudosample as an observation. Genes with a false discovery rate adjusted p-value <.05 were taken as significant (Table S9).

The pseudosampling approach was then repeated to compare *Eed-cKO* cells from Lhx9 and *Glut/GABA* cells against all other *Eed-cKO* cells (Table S10). To identify the *Eed-cKO* genes that were specifically upregulated in the *Eed-cKO* Lhx9 and/or Glut/GABA cells, we then took the overlap between the upregulated genes from comparing Lhx9 and Glut/GABA *Eed-cKO* versus Lhx9 and Glut/GABA control cells, and the DE genes from comparing Lhx9-/Glut/GABA *Eed-cKO* cells versus all other *Eed-cKO* cells (Table S11).

Figure Legends

Figure 1.

Single cell transcriptomic analysis of *Eed-cKO* mutants reveals upregulation of TFs and Hox genes in the hypothalamus.

(A) *In situ* hybridisation of *Foxg1* in cross-section of E15.5 mouse embryo (image from Allen Brain Atlas) (Thompson et al., 2014). The dissected region analysed by scRNA-seq is boxed. (B) Process for quality control and biological filtering of hypothalamic scRNA-seq cells. (C) UMAP of hypothalamic scRNA-seq cells, combined from control and *Eed-cKO*, at E18.5, based upon 300 genes (Table S1). (D-E) UMAP of E18.5 hypothalamic scRNA-seq All-Hypo cells, showing expression of *Cdkn2a* and *Hoxd10*, in control and *Eed-cKO*. (F-G) Violin plots comparing the expression levels of Hox genes (F) and the highest differentially expressed (adjusted p-value $\leq$ 0.05) transcription factors (G) between control and *Eed-cKO*, in E18.5 hypothalamic scRNA-seq All-Hypo cells. Markers below violin plots denote differentially expressed genes; green markers indicate up-regulation in *Eed-cKO*. The shape of markers demarcates the type of differential expression; triangles indicate genes which are generally differentially expressed (DEg, differential expression), squares indicate genes which change in the magnitude of expression (DEm, differential magnitude), and stars indicate genes which change in the number of cells expressing the gene (DEa, differential abundance).

Figure 2.

***Eed-cKO* mutants display more Glut/GABA cells.**

(A-F) UMAP embedding, based upon 300 DE genes (Table S1), of E18.5 All-Hypo cells, showing astrocytes (*Gfap*), oligodendrocyte precursors (*Olig1*), ependymal cells (*Foxj1*), tanycytes (*Rax*), GABAergic neurons (*Slc32a1*) and glutamatergic neurons (*Slc17a6*). (G) Glut/GABA co-expression revealed by *Slc32a1* and *Slc17a6* expression.

Figure 3.

***Eed-cKO* mutants display ectopic Tfap2b expression in the hypothalamus.**

(A-D) Staining for DAPI and Tfap2b in sagittal sections of E18.5 brains, in control and *Eed-cKO*. Dashed squares in (A-B) delineate regions of hypothalamic tissue magnified in (C-D). In control, Tfap2b expression is observed in the mid- and hindbrain regions. In *Eed-cKO* mutants, Tfap2b expression is increased and expands into the anterior brain, including the hypothalamus. (E-F) UMAP embedding of E18.5 hypothalamic scRNA-seq All-Hypo cells, with each cell coloured according to the expression level of *Tfap2b* in control and *Eed-cKO*. Scale bar; 1,000 µm in (A, B), 100 µm in (C, D).

Figure 4.

***Eed-cKO* is necessary for DA, Hcrt and Tac2 cells.**

(A-B) UMAP embedding of hypothalamic NP-DA cells, based on 122 genes (Table S1), in control and *Eed-cKO*, at E18.5. Each cluster is labelled by the combination of NP-DA marker genes upregulated in that cluster. (C) Heatmap displaying average gene expression of the NP-DA marker genes in each UMAP cell cluster, in control (blue) and *Eed-cKO* (pink). Gene expression is measured in log2(CPT+1), scaled between 0 and 1 along each row (see Mat&Met). The *Ddc-Th-Slc6a3*, *Tac2* and *Hcrt* clusters are absent in *Eed-cKO,* and hence a column of 0 expression was depicted. (D) Expression levels of NP-DA marker genes, in control and *Eed-cKO*, at E18.5. Symbols below violin plots indicate differentially expressed genes; green markers show up-regulation in *Eed-cKO* and red indicates down-regulation. The shape of markers demarcates the type of differential expression; triangles indicate genes which are generally differentially expressed (DEg, differential expression, general), squares indicate genes which change in the magnitude of expression (DEm, differential magnitude), and stars indicate genes which change in the number of cells expressing the gene (DEa, differential abundance). See Table S2 for analysis.

Figure 5.

***Eed-cKO* is necessary for DA, *Hcrt* and *Tac2* cells.**

(A-E) UMAP embedding of E18.5 NP-DA cells, based upon 122 DE genes (Table S1), showing expression of *Ddc*, *Th*, *Slc6a3*, *Tac2* and *Hcrt*. (A-C) Two prominent clusters co-express *Ddc-Th-Slc6a3*, and these cluster are largely missing in *Eed-cKO*. (D-E) Similarly, one specific *Tac2* cluster and the *Hcrt* cluster are largely absent in *Eed-cKO* mutants.

Figure 6.

***Eed* is critical for Hcrt neurons.**

(A-B) Staining for DAPI in sagittal sections of E18.5 control and *Eed-cKO* mutant brains. Dashed, square insets delineate the lateral hypothalamus. (C-F) Staining for DAPI and Hcrt in the lateral hypothalamus, in control and *Eed-cKO* embryos. A cluster of Hcrt cells is present in control, while *Eed-cKO* mutants only show occasional, weakly expressing cells. (G-H) UMAP embedding of E18.5 hypothalamic scRNA-seq NP-DA cells, with each cell coloured according to the expression level of *Hcrt* in control and *Eed-cKO*. Scale bar; 500 µm in (A, B), 100 µm in (C-F).

Figure 7.

Developmental onset of Glut/GABA co-expression and loss of Lhx9/Sox2 progenitors.

(A-H) UMAP embedding of hypothalamic cells from E13.5, E15.5 and E18.5. (A-D) Glut/GABA co-expression and Tfap2 expression is limited in control but increases in *Eed-cKO* mutants. (E) High-expression Hcrt cells are not present in *Eed-cKO* mutants. (F-H) In control, a set of *Sox2/Lhx9* progenitor cells are present (green dashed oval), but this cell group is greatly reduced in *Eed-cKO* mutants. (I) Expression analysis of *Lhx9* cells, Glut/GABA cells and "other" cells, at E13.5-E18.5. In *Eed-cKO*, *Lhx9* and Glut/GABA cells show ectopic expression

of a number of developmental TFs, and display upregulation to a greater extent than all "other" cells.

Supplemental Figures and Tables Legends

Supplemental Figure 1.

Eed-cKO mutants display loss of H3K27me3.

(A-D) Sagittal sections of E11.5 control and *Eed-cKO* embryos, stained with DAPI and immunostained for H3K27me3. White dashed line in (D) delineates the CNS in the *Eed-cKO*. In control, H3K27me3 staining is observed throughout the CNS. In *Eed-cKO*, staining is below detection in most parts of the CNS, including in the hypothalamus. A weak signal is apparent in the *Eed-cKO* mutants at the boundary between Tel- and Diencephalon, as well as at the boundary between the Diencephalon and Mid-brain (arrows in D). (E-J) Sagittal sections of E12.5 control and *Eed-cKO* embryos, stained with DAPI and H3K27me3. White, dashed square insets in (G-H) indicate hypothalamic regions in control and *Eed-cKO* magnified in (I) and (J) respectively. Yellow dashed line in H and J delineates the CNS, including the hypothalamic region. In control, H3K27me3 staining is observed throughout the CNS. In *Eed-cKO*, staining is below detection in all parts of the CNS, including in the hypothalamus. Scale bar; 500 μm in (A-H), 200 μm in (I, J).

Supplemental Figure 2.

Eed-cKO mutants display reduced proliferation in the hypothalamus.

(A-H) Staining for Sox2, PH3 and DAPI in sagittal sections of E15.5 embryos, in control and *Eed-cKO*. (A-B) White dashed lines delineate the hypothalamic region used for proliferation analysis. Dashed square insets delineate regions magnified in (C-H). (I, J) Quantification of proliferation in hypothalamic tissue of control vs *Eed-cKO*, at E15.5, plotted as PH3+ cells per mm^3 of DAPI and Sox2 signals respectively, shows reduced proliferation in *Eed-cKO*. (K) Ratios of Sox2/DAPI signal did not change between hypothalamic tissues of control and *Eed-cKO* embryos at E15.5. Student's t-test; mean +/- SEM; n= 3 embryos per genotype, n=9 sections; 3 sections per embryo, per genotype. Scale bar; 200 μm in (A, B), 50 μm in (C-H). For source data, see Table S7.

Supplemental Figure 3.

Technical filtering of scRNA-seq data.

Technical filtering at E18.5 depicts histograms of the Unique Molecular Identifiers (UMIs) expressed per gene, the total UMIs, and the genes expressed across the cells both before (top) and after (bottom) quality control, respectively. The black, red, and orange vertical lines indicate the cut offs used for quality control, the mean for each quality metric, and the median for each quality metric, respectively.

Supplemental Figure 4.

GO analysis of scRNA-seq data.

(A-B) GO analysis of All-Hypo (A) and NP-DA cells (B). The first panel (left) shows the total number of genes up (green) and down (red) for each type of differential expression (DEa, DEg, and DEm) in the *Eed-cKO* (adjusted p-value *<0.05).* The right panel depicts stacked bar charts of the total number of gene sets ("Terms") grouped as "TF activity/DNA binding" if they mention "binding" or "transcription" in the term name, or "H3K27me3", "H3K36me3" or "H3K4me3" if these epigenetic marks were mentioned in the term name; the remaining terms are grouped as "Other". The epigenetic terms indicate genes marked by the respective modification in a biological tissue sample in the *ENCyclopaedia of DNA Elements* (ENCODE.

Supplemental Figure 5.

***Eed-cKO* mutants display ectopic Pax2 expression in the hypothalamus.**

(A-D) Staining for Pax2 and DAPI in sagittal sections of E18.5 brains, in control and *Eed-cKO*. In control, Pax2 is expressed in the mid- and hindbrain. In contrast, *Eed-cKO* mutants display ectopic Pax2 expression in all anterior regions of the brain, including the hypothalamus. (E-F) UMAP embedding of E18.5 hypothalamic scRNA-seq data for the All-Hypo cells, with each cell coloured according to the expression levels of Pax2, in control and *Eed-cKO*. Scale bar; 500 μm in (A-D).

Supplemental Figure 6.

***Eed-cKO* mutants display Hox and posterior TF expression in the hypothalamus.**

(A-B) Heatmap displaying average gene expression of the Hox and posterior TF genes in each UMAP cell cluster, in control (blue) and *Eed-cKO* (pink). Gene expression is measured in log2(CPT+1), scaled between 0 and 1 along each row. The *Ddc-Th-Slc6a3*, *Tac2* and *Hcrt* clusters are absent in *Eed-cKO,* and hence a column of 0 expression was depicted.

Supplemental Figure 7.

***Eed* is not critical for the generation of Avp neurons.**

(A-B) Staining for Avp and DAPI in sagittal sections of E18.5 control and *Eed-cKO* mutant brains. Dashed, square insets delineate Avp cells in dorsal and ventral hypothalamic regions. (C-F) Avp+ cells in dorsal (d-Hy) and ventral (v-Hy) regions of hypothalamus in control and *Eed-cKO* embryos. The organization and clustering of v-Hy region Avp cells appear to be disrupted in *Eed-cKO*. (G-H) UMAP embedding of E18.5 hypothalamic scRNA-seq NP-DA cells, with each cell coloured according to the expression level of *Avp* in control and *Eed-cKO*. Scale bar; 1000 μm in (A, B), 100 μm in (C-F).

Supplemental Figure 8.

***Eed-cKO* is not necessary for most NP-DA cell fates.**

UMAP embedding of E18.5 NP-DA cells, based upon 122 DE genes (Table S1), showing expression of neuropeptide genes, in control and *Eed-cKO* cells.

Supplemental Figure 9.

***Eed-cKO* is not necessary for most NP-DA cell fates.**

UMAP embedding of E18.5 NP-DA cells, based upon 122 DE genes (Table S1), showing expression of neuropeptide genes, in control and *Eed-cKO* cells.

Supplemental Figure 10.

Technical filtering and analysis of E13.5 and E15.5 scRNA-seq data.

(A-B) Technical filtering depicts histograms of the Unique Molecular Identifiers (UMIs) expressed per gene, the total UMIs, and the genes expressed across the cells both before and after quality control, respectively. The black, red, and orange vertical lines indicate the cut offs used for quality control, the mean for each quality metric, and the median for each quality metric, respectively. (C) UMAP embedding of E13.5, E15.5 and E18.5 cells, showing that all of the major cell types are generated in the hypothalamus in *Eed-cKO* mutants. However, DA (*Slc6a3*) and a subset of *Tac2* cells are missing.

Supplemental Table 1.

Gene lists for UMAP embedding.

Gene lists for UMAP embedding of All-Hypo and NP-DA cells.

Supplemental Table 2.

Differential expression in the All-Hypo and NP-DA cells.

Differential expression in All-Hypo and NP-DA cells, when comparing single-cell transcriptomic data between control and *Eed-cKO*, at E18.5.

Supplemental Table 3.

Gene Ontology analysis of All-hypo cells.

Gene Ontology analysis of DE genes in All-Hypo cells, at E18.5, showing enrichment of TF activity/DNA binding, H3K27me3 and H3K36me3.

Supplemental Table 4.

Gene Ontology analysis of NP-DA cells.

Gene Ontology analysis of DE genes in NP-DA cells, at E18.5, showing enrichment of TF activity/DNA binding, H3K27me3 and H3K36me3.

Supplemental Table 5.

Differential expression in NP-DA cell clusters.
Differential expression in NP-DA cell clusters, at E18.5, in control and *Eed-cKO*.

Supplemental Table 6.

Temporal onset of NP-DA genes and the effects in *Eed-cKO*.
Developmental onset of the NP-DA marker genes, based on the Allen Brain Atlas (ABA) (Thompson et al., 2014) and the literature (Diaz et al., 2014; Knoll et al., 2013). Light red depicts weak expression or expression in sub-regions of the hypothalamus.

Supplemental Table 7.

Source Data for Figure S2
Data and analysis quantifying proliferation in *Eed-cKO* & control.

Supplemental Table 8.

Marker genes used for broad labelling of early time points and confusion matrix from logistic regression classification.
Relevant information for labelling the cell types for the early time points.

Supplemental Table 9.

Differential expression between *Eed-cKO* and control in Lhx9 and Glut/GABA cells.
Differentially expressed gene lists and associated statistics from comparing selected subsets of *Eed-cKO* cells against control from E13.5, E15.5, and E18.5. Lhx9 *Eed-cKO* cells were compared against Lhx9 control cells, and Glut/GABA *Eed-cKO* cells were compared against Glut/GABA control cells.

Supplemental Table 10.

Differential expression between *Eed-cKO* Lhx9 and Glut/GABA cells against all other *Eed-cKO* cells.
Differentially expressed gene lists and associated statistics from comparing selected subsets of *Eed-cKO* cells against the all other *Eed-cKO* cells from E13.5, E15.5, and E18.5. Lhx9 *Eed-cKO* cells were compared against all other *Eed-cKO* cells (excluding Glut/GABA *Eed-cKO*), and Glut/GABA *Eed-cKO* cells were compared against all other *Eed-cKO* cells (excluding Lhx9 *Eed-cKO*).

Supplemental Table 11.

Genes differentially effected in Lhx9 and Glut/GABA *Eed-cKO* cells but not other cells.
Overlap of the gene lists from comparing Lhx9 *Eed-cKO* versus control and Lhx9 *Eed-cKO* cells versus all other *Eed-cKO* cells. Also overlap genes from comparing Glut/GABA *Eed-cKO* versus control and Glut/GABA *Eed-cKO* cells versus all other *Eed-cKO* cells. These genes thereby

represent those which were significantly *Eed-cKO* effected in these cell subsets but not all other cells.

REFERENCES

Abed, J.A., and Jones, R.S. (2012). H3K36me3 key to Polycomb-mediated gene silencing in lineage specification. Nat Struct Mol Biol *19*, 1214-1215.

Alpar, A., Benevento, M., Romanov, R.A., Hokfelt, T., and Harkany, T. (2019). Hypothalamic cell diversity: non-neuronal codes for long-distance volume transmission by neuropeptides. Curr Opin Neurobiol *56*, 16-23.

Alvarez-Bolado, G. (2019). Development of neuroendocrine neurons in the mammalian hypothalamus. Cell Tissue Res *375*, 23-39.

Arcipowski, K.M., Martinez, C.A., and Ntziachristos, P. (2016). Histone demethylases in physiology and cancer: a tale of two enzymes, JMJD3 and UTX. Curr Opin Genet Dev *36*, 59-67.

Aylwin, C.F., Vigh-Conrad, K., and Lomniczi, A. (2019). The Emerging Role of Chromatin Remodeling Factors in Female Pubertal Development. Neuroendocrinology *109*, 208-217.

Bahrampour, S., Jonsson, C., and Thor, S. (2019). Brain expansion promoted by polycomb-mediated anterior enhancement of a neural stem cell proliferation program. PLoS Biol *17*, e3000163.

Banaszynski, L.A., Wen, D., Dewell, S., Whitcomb, S.J., Lin, M., Diaz, N., Elsasser, S.J., Chapgier, A., Goldberg, A.D., Canaani, E.*, et al.* (2013). Hira-dependent histone H3.3 deposition facilitates PRC2 recruitment at developmental loci in ES cells. Cell *155*, 107-120.

Bedont, J.L., Newman, E.A., and Blackshaw, S. (2015). Patterning, specification, and differentiation in the developing hypothalamus. Wiley Interdiscip Rev Dev Biol *4*, 445-468.

Biran, J., Tahor, M., Wircer, E., and Levkowitz, G. (2015). Role of developmental factors in hypothalamic function. Front Neuroanat *9*, 47.

Bjorklund, A., and Dunnett, S.B. (2007). Dopamine neuron systems in the brain: an update. Trends Neurosci *30*, 194-202.

Blackshaw, S., Scholpp, S., Placzek, M., Ingraham, H., Simerly, R., and Shimogori, T. (2010). Molecular pathways controlling development of thalamus and hypothalamus: from neural specification to circuit formation. J Neurosci *30*, 14925-14930.

Burbridge, S., Stewart, I., and Placzek, M. (2016). Development of the Neuroendocrine Hypothalamus. Compr Physiol *6*, 623-643.

Burgold, T., Spreafico, F., De Santa, F., Totaro, M.G., Prosperini, E., Natoli, G., and Testa, G. (2008). The histone H3 lysine 27-specific demethylase Jmjd3 is required for neural commitment. PLoS One *3*, e3034.

Burkardt, D.D., Tatton-Brown, K., Dobyns, W., and Graham, J.M., Jr. (2019). Approach to overgrowth syndromes in the genome era. Am J Med Genet C Semin Med Genet *181*, 483-490.

Campbell, J.N., Macosko, E.Z., Fenselau, H., Pers, T.H., Lyubetskaya, A., Tenen, D., Goldman, M., Verstegen, A.M., Resch, J.M., McCarroll, S.A.*, et al.* (2017). A molecular census of arcuate hypothalamus and median eminence cell types. Nat Neurosci *20*, 484-496.

Caviness, V.S., Jr., Takahashi, T., and Nowakowski, R.S. (1995). Numbers, time and neocortical neuronogenesis: a general developmental and evolutionary model. Trends Neurosci *18*, 379-383.

Chammas, P., Mocavini, I., and Di Croce, L. (2020). Engaging chromatin: PRC2 structure meets function. Br J Cancer *122*, 315-328.

Chen, R., Wu, X., Jiang, L., and Zhang, Y. (2017). Single-Cell RNA-Seq Reveals Hypothalamic Cell Diversity. Cell Rep *18*, 3227-3241.

Clapcote, S.J., and Roder, J.C. (2005). Simplex PCR assay for sex determination in mice. Biotechniques *38*, 702, 704, 706.

Coleman, R.T., and Struhl, G. (2017). Causal role for inheritance of H3K27me3 in maintaining the OFF state of a Drosophila HOX gene. Science *356*.
Cyrus, S., Burkardt, D., Weaver, D.D., and Gibson, W.T. (2019). PRC2-complex related dysfunction in overgrowth syndromes: A review of EZH2, EED, and SUZ12 and their syndromic phenotypes. Am J Med Genet C Semin Med Genet *181*, 519-531.
Dalal, J., Roh, J.H., Maloney, S.E., Akuffo, A., Shah, S., Yuan, H., Wamsley, B., Jones, W.B., de Guzman Strong, C., Gray, P.A.*, et al.* (2013). Translational profiling of hypocretin neurons identifies candidate molecules for sleep regulation. Genes Dev *27*, 565-578.
Davis, C.A., Hitz, B.C., Sloan, C.A., Chan, E.T., Davidson, J.M., Gabdank, I., Hilton, J.A., Jain, K., Baymuradov, U.K., Narayanan, A.K.*, et al.* (2018). The Encyclopedia of DNA elements (ENCODE): data portal update. Nucleic Acids Res *46*, D794-D801.
De La Herran-Arita, A.K., Zomosa-Signoret, V.C., Millan-Aldaco, D.A., Palomero-Rivero, M., Guerra-Crespo, M., Drucker-Colin, R., and Vidaltamayo, R. (2011). Aspects of the narcolepsy-cataplexy syndrome in O/E3-null mutant mice. Neuroscience *183*, 134-143.
De Zegher, F., Van Den Berghe, G., Devlieger, H., Eggermont, E., and Veldhuis, J.D. (1993). Dopamine inhibits growth hormone and prolactin secretion in the human newborn. Pediatr Res *34*, 642-645.
Diaz, C., Morales-Delgado, N., and Puelles, L. (2014). Ontogenesis of peptidergic neurons within the genoarchitectonic map of the mouse hypothalamus. Front Neuroanat *8*, 162.
Economides, K.D., Zeltser, L., and Capecchi, M.R. (2003). Hoxb13 mutations cause overgrowth of caudal spinal cord and tail vertebrae. Dev Biol *256*, 317-330.
Faust, C., Lawson, K.A., Schork, N.J., Thiel, B., and Magnuson, T. (1998). The Polycomb-group gene eed is required for normal morphogenetic movements during gastrulation in the mouse embryo. Development *125*, 4495-4506.
Faust, C., Schumacher, A., Holdener, B., and Magnuson, T. (1995). The eed mutation disrupts anterior mesoderm production in mice. Development (Cambridge, England) *121*, 273-285.
Ferran, J.L., Puelles, L., and Rubenstein, J.L. (2015). Molecular codes defining rostrocaudal domains in the embryonic mouse hypothalamus. Front Neuroanat *9*, 46.
Finogenova, K., Bonnet, J., Poepsel, S., Schafer, I.B., Finkl, K., Schmid, K., Litz, C., Strauss, M., Benda, C., and Muller, J. (2020). Structural basis for PRC2 decoding of active histone methylation marks H3K36me2/3. Elife *9*.
Henry, F.E., Sugino, K., Tozer, A., Branco, T., and Sternson, S.M. (2015). Cell type-specific transcriptomics of hypothalamic energy-sensing neuron responses to weight-loss. Elife *4*.
Huisman, C., Cho, H., Brock, O., Lim, S.J., Youn, S.M., Park, Y., Kim, S., Lee, S.K., Delogu, A., and Lee, J.W. (2019). Single cell transcriptome analysis of developing arcuate nucleus neurons uncovers their key developmental regulators. Nat Commun *10*, 3696.
Huisman, C., Kim, Y.A., Jeon, S., Shin, B., Choi, J., Lim, S.J., Youn, S.M., Park, Y., K, C.M., Kim, S.*, et al.* (2021). The histone H3-lysine 4-methyltransferase Mll4 regulates the development of growth hormone-releasing hormone-producing neurons in the mouse hypothalamus. Nat Commun *12*, 256.
Isono, K., Fujimura, Y., Shinga, J., Yamaki, M., J, O.W., Takihara, Y., Murahashi, Y., Takada, Y., Mizutani-Koseki, Y., and Koseki, H. (2005). Mammalian polyhomeotic homologues Phc2 and Phc1 act in synergy to mediate polycomb repression of Hox genes. Mol Cell Biol *25*, 6694-6706.

Jadhav, U., Manieri, E., Nalapareddy, K., Madha, S., Chakrabarti, S., Wucherpfennig, K., Barefoot, M., and Shivdasani, R.A. (2020). Replicational Dilution of H3K27me3 in Mammalian Cells and the Role of Poised Promoters. Mol Cell *78*, 141-151 e145.
Jeong, J.H., Woo, Y.J., Chua, S., Jr., and Jo, Y.H. (2016). Single-Cell Gene Expression Analysis of Cholinergic Neurons in the Arcuate Nucleus of the Hypothalamus. PLoS One *11*, e0162839.
Karczewski, K.J., Francioli, L.C., Tiao, G., Cummings, B.B., Alfoldi, J., Wang, Q., Collins, R.L., Laricchia, K.M., Ganna, A., Birnbaum, D.P.*, et al.* (2020). The mutational constraint spectrum quantified from variation in 141,456 humans. Nature *581*, 434-443.
Kim, D.W., Washington, P.W., Wang, Z.Q., Lin, S.H., Sun, C., Ismail, B.T., Wang, H., Jiang, L., and Blackshaw, S. (2020). The cellular and molecular landscape of hypothalamic patterning and differentiation from embryonic to late postnatal development. Nat Commun *11*, 4360.
Kim, D.W., Yao, Z., Graybuck, L.T., Kim, T.K., Nguyen, T.N., Smith, K.A., Fong, O., Yi, L., Koulena, N., Pierson, N.*, et al.* (2019). Multimodal Analysis of Cell Types in a Hypothalamic Node Controlling Social Behavior. Cell *179*, 713-728 e717.
Knoll, J.G., Clay, C.M., Bouma, G.J., Henion, T.R., Schwarting, G.A., Millar, R.P., and Tobet, S.A. (2013). Developmental profile and sexually dimorphic expression of kiss1 and kiss1r in the fetal mouse brain. Front Endocrinol (Lausanne) *4*, 140.
Kurrasch, D.M., Cheung, C.C., Lee, F.Y., Tran, P.V., Hata, K., and Ingraham, H.A. (2007). The neonatal ventromedial hypothalamus transcriptome reveals novel markers with spatially distinct patterning. J Neurosci *27*, 13624-13634.
Lam, B.Y.H., Cimino, I., Polex-Wolf, J., Nicole Kohnke, S., Rimmington, D., Iyemere, V., Heeley, N., Cossetti, C., Schulte, R., Saraiva, L.R.*, et al.* (2017). Heterogeneity of hypothalamic pro-opiomelanocortin-expressing neurons revealed by single-cell RNA sequencing. Mol Metab *6*, 383-392.
Laprell, F., Finkl, K., and Muller, J. (2017). Propagation of Polycomb-repressed chromatin requires sequence-specific recruitment to DNA. Science *356*, 85-88.
Laugesen, A., Hojfeldt, J.W., and Helin, K. (2019). Molecular Mechanisms Directing PRC2 Recruitment and H3K27 Methylation. Mol Cell *74*, 8-18.
Li, X., Isono, K., Yamada, D., Endo, T.A., Endoh, M., Shinga, J., Mizutani-Koseki, Y., Otte, A.P., Casanova, M., Kitamura, H.*, et al.* (2011). Mammalian polycomb-like Pcl2/Mtf2 is a novel regulatory component of PRC2 that can differentially modulate polycomb activity both at the Hox gene cluster and at Cdkn2a genes. Mol Cell Biol *31*, 351-364.
Liu, J., Merkle, F.T., Gandhi, A.V., Gagnon, J.A., Woods, I.G., Chiu, C.N., Shimogori, T., Schier, A.F., and Prober, D.A. (2015). Evolutionarily conserved regulation of hypocretin neuron specification by Lhx9. Development *142*, 1113-1124.
Lomniczi, A., Loche, A., Castellano, J.M., Ronnekleiv, O.K., Bosch, M., Kaidar, G., Knoll, J.G., Wright, H., Pfeifer, G.P., and Ojeda, S.R. (2013). Epigenetic control of female puberty. Nat Neurosci *16*, 281-289.
Miao, Z., Deng, K., Wang, X., and Zhang, X. (2018). DEsingle for detecting three types of differential expression in single-cell RNA-seq data. Bioinformatics *34*, 3223-3224.
Mickelsen, L.E., Bolisetty, M., Chimileski, B.R., Fujita, A., Beltrami, E.J., Costanzo, J.T., Naparstek, J.R., Robson, P., and Jackson, A.C. (2019). Single-cell transcriptomic analysis of the lateral hypothalamic area reveals molecularly distinct populations of inhibitory and excitatory neurons. Nat Neurosci *22*, 642-656.
Mickelsen, L.E., Kolling, F.W.t., Chimileski, B.R., Fujita, A., Norris, C., Chen, K., Nelson, C.E., and Jackson, A.C. (2017). Neurochemical Heterogeneity Among Lateral Hypothalamic

Hypocretin/Orexin and Melanin-Concentrating Hormone Neurons Identified Through Single-Cell Gene Expression Analysis. eNeuro *4*.
Mocavini, I., and Di Croce, L. (2020). RNA closing the Polycomb circle. Nat Genet *52*, 866-867.
Moffitt, J.R., Bambah-Mukku, D., Eichhorn, S.W., Vaughn, E., Shekhar, K., Perez, J.D., Rubinstein, N.D., Hao, J., Regev, A., Dulac, C.*, et al.* (2018). Molecular, spatial, and functional single-cell profiling of the hypothalamic preoptic region. Science *362*.
Monedero Cobeta, I., Salmani, B.Y., and Thor, S. (2017). Anterior-Posterior Gradient in Neural Stem and Daughter Cell Proliferation Governed by Spatial and Temporal Hox Control. Curr Biol *27*, 1161-1172.
Montgomery, N.D., Yee, D., Chen, A., Kalantry, S., Chamberlain, S.J., Otte, A.P., and Magnuson, T. (2005). The murine polycomb group protein Eed is required for global histone H3 lysine-27 methylation. Curr Biol *15*, 942-947.
Nesan, D., and Kurrasch, D.M. (2016). Genetic programs of the developing tuberal hypothalamus and potential mechanisms of their disruption by environmental factors. Mol Cell Endocrinol *438*, 3-17.
Orquera, D.P., Nasif, S., Low, M.J., Rubinstein, M., and de Souza, F.S.J. (2016). Essential function of the transcription factor Rax in the early patterning of the mammalian hypothalamus. Dev Biol *416*, 212-224.
Park, D.H., Hong, S.J., Salinas, R.D., Liu, S.J., Sun, S.W., Sgualdino, J., Testa, G., Matzuk, M.M., Iwamori, N., and Lim, D.A. (2014). Activation of neuronal gene expression by the JMJD3 demethylase is required for postnatal and adult brain neurogenesis. Cell Rep *8*, 1290-1299.
Pevny, L.H., Sockanathan, S., Placzek, M., and Lovell-Badge, R. (1998). A role for SOX1 in neural determination. Development *125*, 1967-1978.
Piunti, A., and Shilatifard, A. (2016). Epigenetic balance of gene expression by Polycomb and COMPASS families. Science *352*, aad9780.
Pliner, H.A., Shendure, J., and Trapnell, C. (2019). Supervised classification enables rapid annotation of cell atlases. Nat Methods *16*, 983-986.
Puelles, L., and Rubenstein, J.L. (2015). A new scenario of hypothalamic organization: rationale of new hypotheses introduced in the updated prosomeric model. Front Neuroanat *9*, 27.
Romanov, R.A., Alpar, A., Hokfelt, T., and Harkany, T. (2019). Unified Classification of Molecular, Network, and Endocrine Features of Hypothalamic Neurons. Annu Rev Neurosci *42*, 1-26.
Romanov, R.A., Tretiakov, E.O., Kastriti, M.E., Zupancic, M., Haring, M., Korchynska, S., Popadin, K., Benevento, M., Rebernik, P., Lallemend, F.*, et al.* (2020). Molecular design of hypothalamus development. Nature.
Romanov, R.A., Zeisel, A., Bakker, J., Girach, F., Hellysaz, A., Tomer, R., Alpar, A., Mulder, J., Clotman, F., Keimpema, E.*, et al.* (2017). Molecular interrogation of hypothalamic organization reveals distinct dopamine neuronal subtypes. Nat Neurosci *20*, 176-188.
Saper, C.B., and Lowell, B.B. (2014). The hypothalamus. Curr Biol *24*, R1111-1116.
Schindelin, J., Arganda-Carreras, I., Frise, E., Kaynig, V., Longair, M., Pietzsch, T., Preibisch, S., Rueden, C., Saalfeld, S., Schmid, B.*, et al.* (2012). Fiji: an open-source platform for biological-image analysis. Nat Methods *9*, 676-682.
Schindelin, J., Rueden, C.T., Hiner, M.C., and Eliceiri, K.W. (2015). The ImageJ ecosystem: An open platform for biomedical image analysis. Mol Reprod Dev *82*, 518-529.
Schmid, B., Schindelin, J., Cardona, A., Longair, M., and Heisenberg, M. (2010). A high-level 3D visualization API for Java and ImageJ. BMC Bioinformatics *11*, 274.

Schumacher, A., Faust, C., and Magnuson, T. (1996). Positional cloning of a global regulator of anterior-posterior patterning in mice. Nature *384*, 648.
Shalev, D., and Melamed, P. (2020). The role of the hypothalamus and pituitary epigenomes in central activation of the reproductive axis at puberty. Mol Cell Endocrinol *518*, 111031.
Shimogori, T., Lee, D.A., Miranda-Angulo, A., Yang, Y., Wang, H., Jiang, L., Yoshida, A.C., Kataoka, A., Mashiko, H., Avetisyan, M.*, et al.* (2010). A genomic atlas of mouse hypothalamic development. Nat Neurosci *13*, 767-775.
Sokolowski, K., Esumi, S., Hirata, T., Kamal, Y., Tran, T., Lam, A., Oboti, L., Brighthaupt, S.C., Zaghlula, M., Martinez, J.*, et al.* (2015). Specification of select hypothalamic circuits and innate behaviors by the embryonic patterning gene dbx1. Neuron *86*, 403-416.
Steffen, P.A., and Ringrose, L. (2014). What are memories made of? How Polycomb and Trithorax proteins mediate epigenetic memory. Nat Rev Mol Cell Biol *15*, 340-356.
Struhl, G. (1983). Role of the esc+ gene product in ensuring the selective expression of segment-specific homeotic genes in Drosophila. J Embryol Exp Morphol *76*, 297-331.
Struhl, G., and Akam, M. (1985). Altered distributions of Ultrabithorax transcripts in extra sex combs mutant embryos of Drosophila. EMBO J *4*, 3259-3264.
Suzuki, M., Mizutani-Koseki, Y., Fujimura, Y., Miyagishima, H., Kaneko, T., Takada, Y., Akasaka, T., Tanzawa, H., Takihara, Y., Nakano, M.*, et al.* (2002). Involvement of the Polycomb-group gene Ring1B in the specification of the anterior-posterior axis in mice. Development *129*, 4171-4183.
Takahashi, T., Nowakowski, R.S., and Caviness, V.S., Jr. (1995). The cell cycle of the pseudostratified ventricular epithelium of the embryonic murine cerebral wall. J Neurosci *15*, 6046-6057.
Takashima, Y., Era, T., Nakao, K., Kondo, S., Kasuga, M., Smith, A.G., and Nishikawa, S. (2007). Neuroepithelial cells supply an initial transient wave of MSC differentiation. Cell *129*, 1377-1388.
Tang, Q.Y., Zhang, S.F., Dai, S.K., Liu, C., Wang, Y.Y., Du, H.Z., Teng, Z.Q., and Liu, C.M. (2020). UTX Regulates Human Neural Differentiation and Dendritic Morphology by Resolving Bivalent Promoters. Stem Cell Reports.
Telley, L., Agirman, G., Prados, J., Amberg, N., Fievre, S., Oberst, P., Bartolini, G., Vitali, I., Cadilhac, C., Hippenmeyer, S.*, et al.* (2019). Temporal patterning of apical progenitors and their daughter neurons in the developing neocortex. Science *364*.
Thompson, C.L., Ng, L., Menon, V., Martinez, S., Lee, C.K., Glattfelder, K., Sunkin, S.M., Henry, A., Lau, C., Dang, C.*, et al.* (2014). A high-resolution spatiotemporal atlas of gene expression of the developing mouse brain. Neuron *83*, 309-323.
Van den Berghe, G., de Zegher, F., and Lauwers, P. (1994a). Dopamine suppresses pituitary function in infants and children. Crit Care Med *22*, 1747-1753.
Van den Berghe, G., de Zegher, F., Lauwers, P., and Veldhuis, J.D. (1994b). Growth hormone secretion in critical illness: effect of dopamine. J Clin Endocrinol Metab *79*, 1141-1146.
van Mierlo, G., Veenstra, G.J.C., Vermeulen, M., and Marks, H. (2019). The Complexity of PRC2 Subcomplexes. Trends Cell Biol *29*, 660-671.
Wang, J., Mager, J., Schnedier, E., and Magnuson, T. (2002). The mouse PcG gene eed is required for Hox gene repression and extraembryonic development. Mamm Genome *13*, 493-503.

Wijayatunge, R., Liu, F., Shpargel, K.B., Wayne, N.J., Chan, U., Boua, J.V., Magnuson, T., and West, A.E. (2018). The histone demethylase Kdm6b regulates a mature gene expression program in differentiating cerebellar granule neurons. Mol Cell Neurosci *87*, 4-17.

Xie, H., Xu, J., Hsu, J.H., Nguyen, M., Fujiwara, Y., Peng, C., and Orkin, S.H. (2014). Polycomb repressive complex 2 regulates normal hematopoietic stem cell function in a developmental-stage-specific manner. Cell Stem Cell *14*, 68-80.

Xie, Y., and Dorsky, R.I. (2017). Development of the hypothalamus: conservation, modification and innovation. Development *144*, 1588-1599.

Yaghmaeian Salmani, B. (2018). Genetic mechanisms regulating the spatio-temporal modulation of proliferation rate and mode in neural progenitors and daughter cells during CNS development. Linkoping University medical Dissertations *No 1628*, 1-63.

Yaghmaeian Salmani, B., Monedero Cobeta, I., Rakar, J., Bauer, S., Curt, J.R., Starkenberg, A., and Thor, S. (2018). Evolutionarily conserved anterior expansion of the central nervous system promoted by a common PcG-Hox program. Development *145*.

Yee, C.L., Wang, Y., Anderson, S., Ekker, M., and Rubenstein, J.L. (2009). Arcuate nucleus expression of NKX2.1 and DLX and lineages expressing these transcription factors in neuropeptide Y(+), proopiomelanocortin(+), and tyrosine hydroxylase(+) neurons in neonatal and adult mice. J Comp Neurol *517*, 37-50.

Zainolabidin, N., Kamath, S.P., Thanawalla, A.R., and Chen, A.I. (2017). Distinct Activities of Tfap2A and Tfap2B in the Specification of GABAergic Interneurons in the Developing Cerebellum. Front Mol Neurosci *10*, 281.

Zeisel, A., Hochgerner, H., Lonnerberg, P., Johnsson, A., Memic, F., van der Zwan, J., Haring, M., Braun, E., Borm, L.E., La Manno, G.*, et al.* (2018). Molecular Architecture of the Mouse Nervous System. Cell *174*, 999-1014 e1022.

Zeisel, A., Munoz-Manchado, A.B., Codeluppi, S., Lonnerberg, P., La Manno, G., Jureus, A., Marques, S., Munguba, H., He, L., Betsholtz, C.*, et al.* (2015). Brain structure. Cell types in the mouse cortex and hippocampus revealed by single-cell RNA-seq. Science *347*, 1138-1142.

Zhang, Y.H., Xu, M., Shi, X., Sun, X.L., Mu, W., Wu, H., Wang, J., Li, S., Su, P., Gong, L.*, et al.* (2021). Cascade diversification directs generation of neuronal diversity in the hypothalamus. Cell Stem Cell.

Zhou, X., Zhong, S., Peng, H., Liu, J., Ding, W., Sun, L., Ma, Q., Liu, Z., Chen, R., Wu, Q.*, et al.* (2020). Cellular and molecular properties of neural progenitors in the developing mammalian hypothalamus. Nat Commun *11*, 4063.

Figure 1

Sc-RNA-seq analysis of *Eed-cKO* mutants

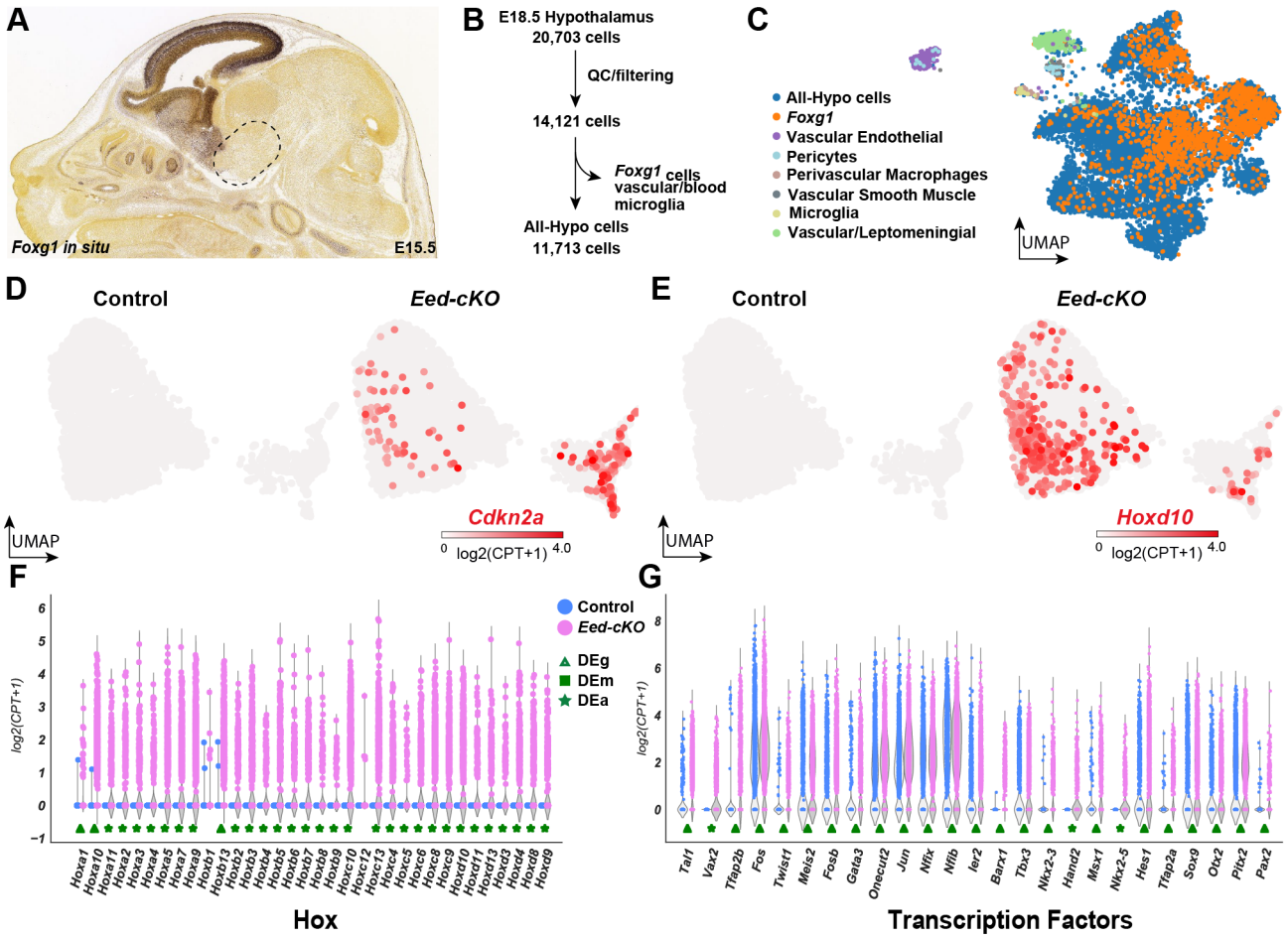

Figure 2

Eed mutants display more Glut/GABA cells

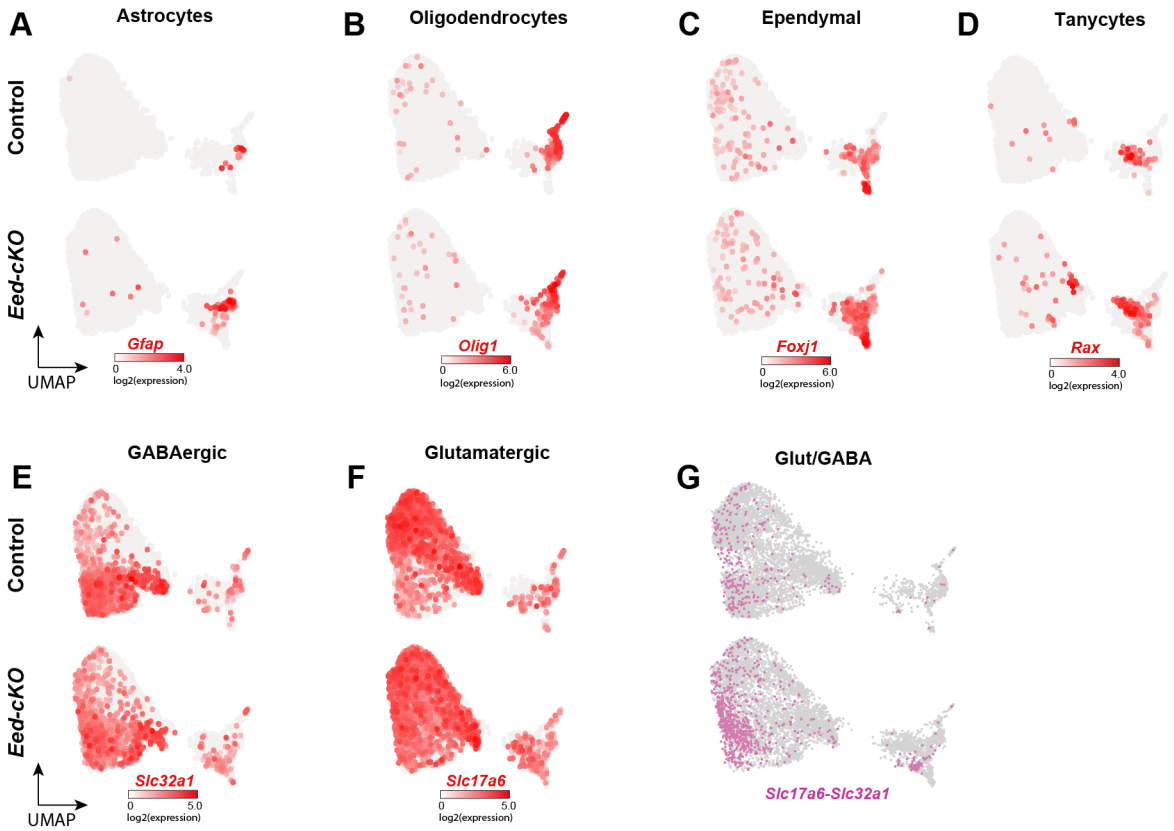

Figure 3

Eed-cKO mutants display ectopic TFAP2b expression

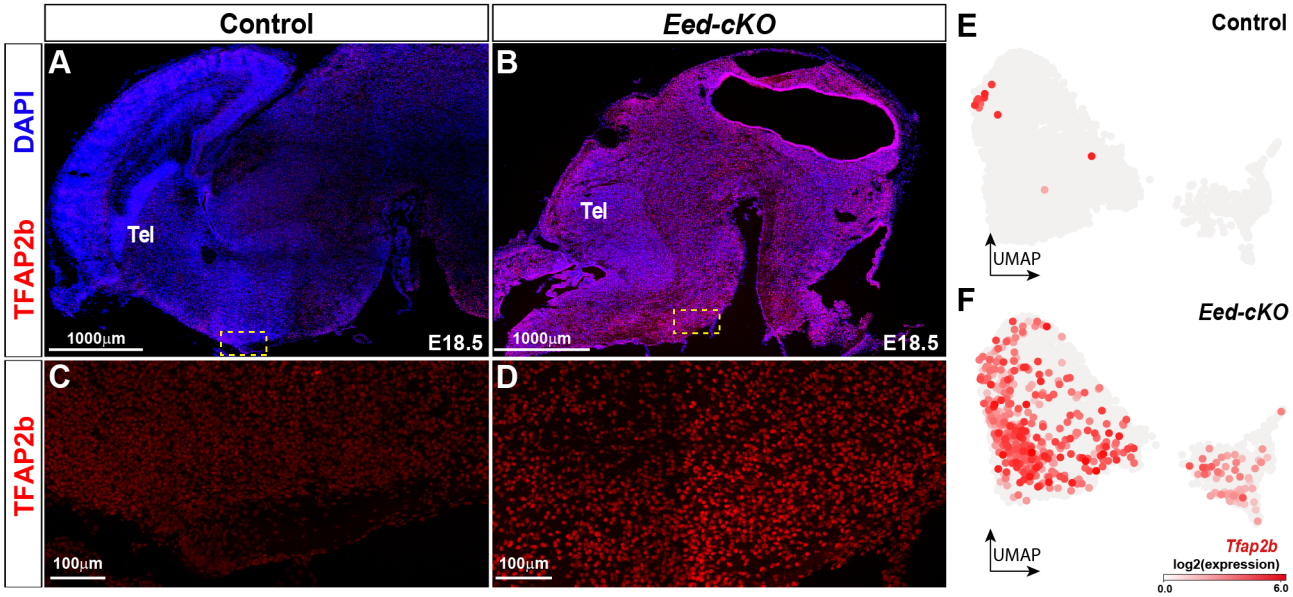

Figure 4

Eed is necessary for Dopamine, Hcrt and Tac2 cells

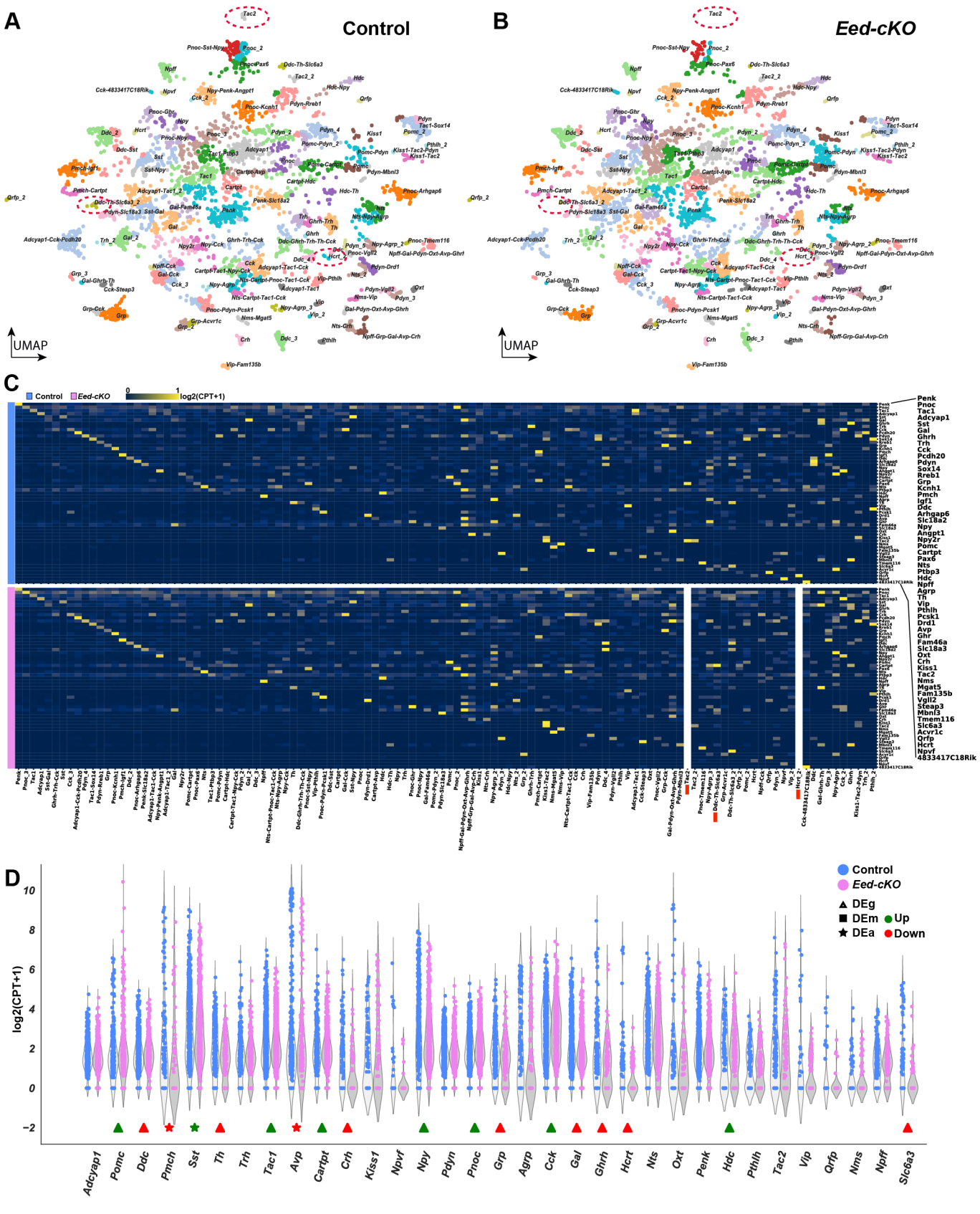

Figure 5

Eed is necessary for Dopamine, Hcrt and Tac2 cells

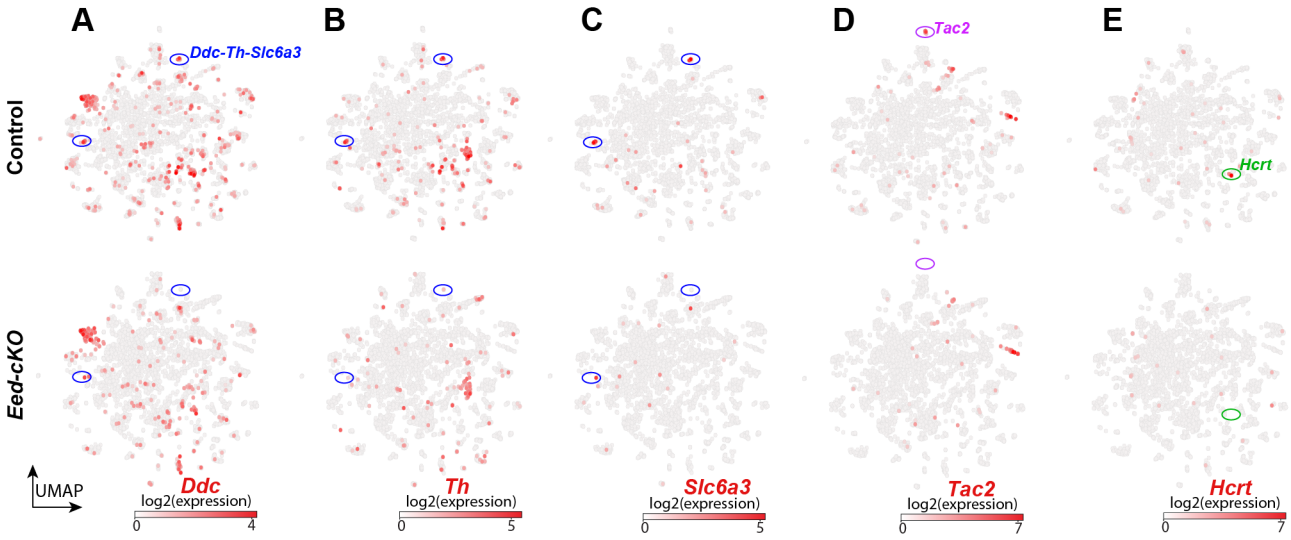

Figure 6

Eed is critical for Hcrt neurons

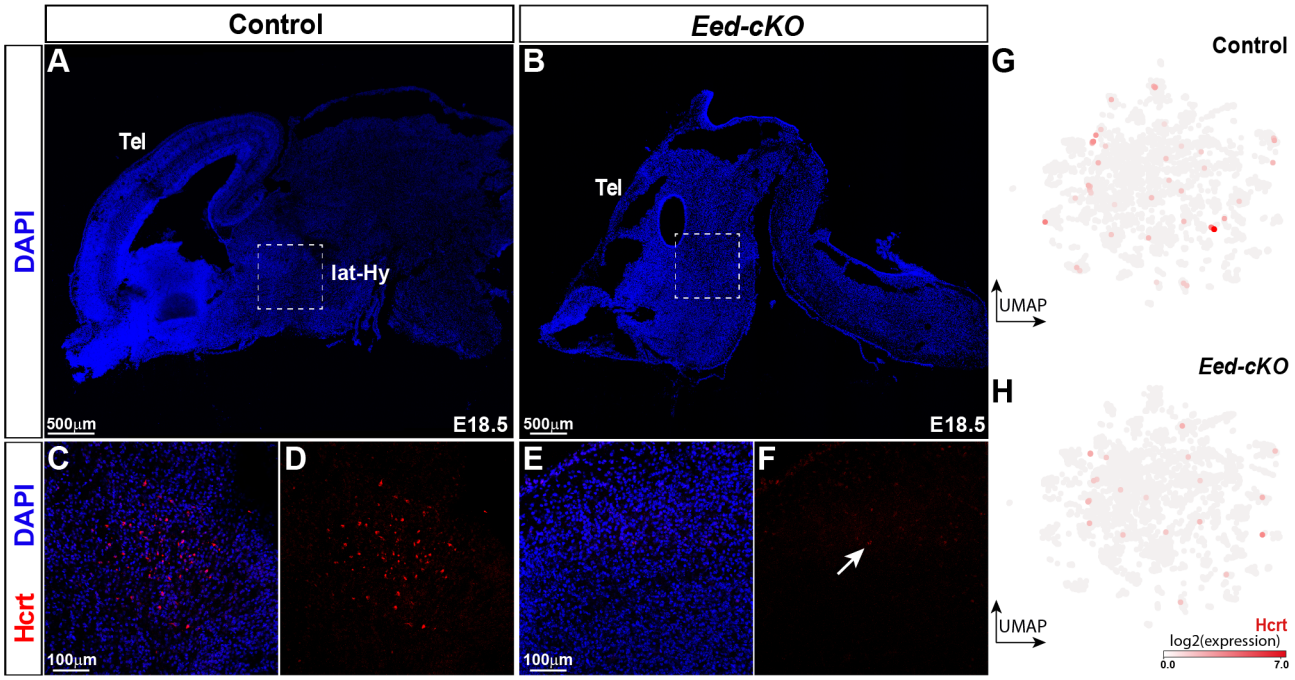

Figure 7

Glut/GABA co-expression and loss of Lhx9 progenitors

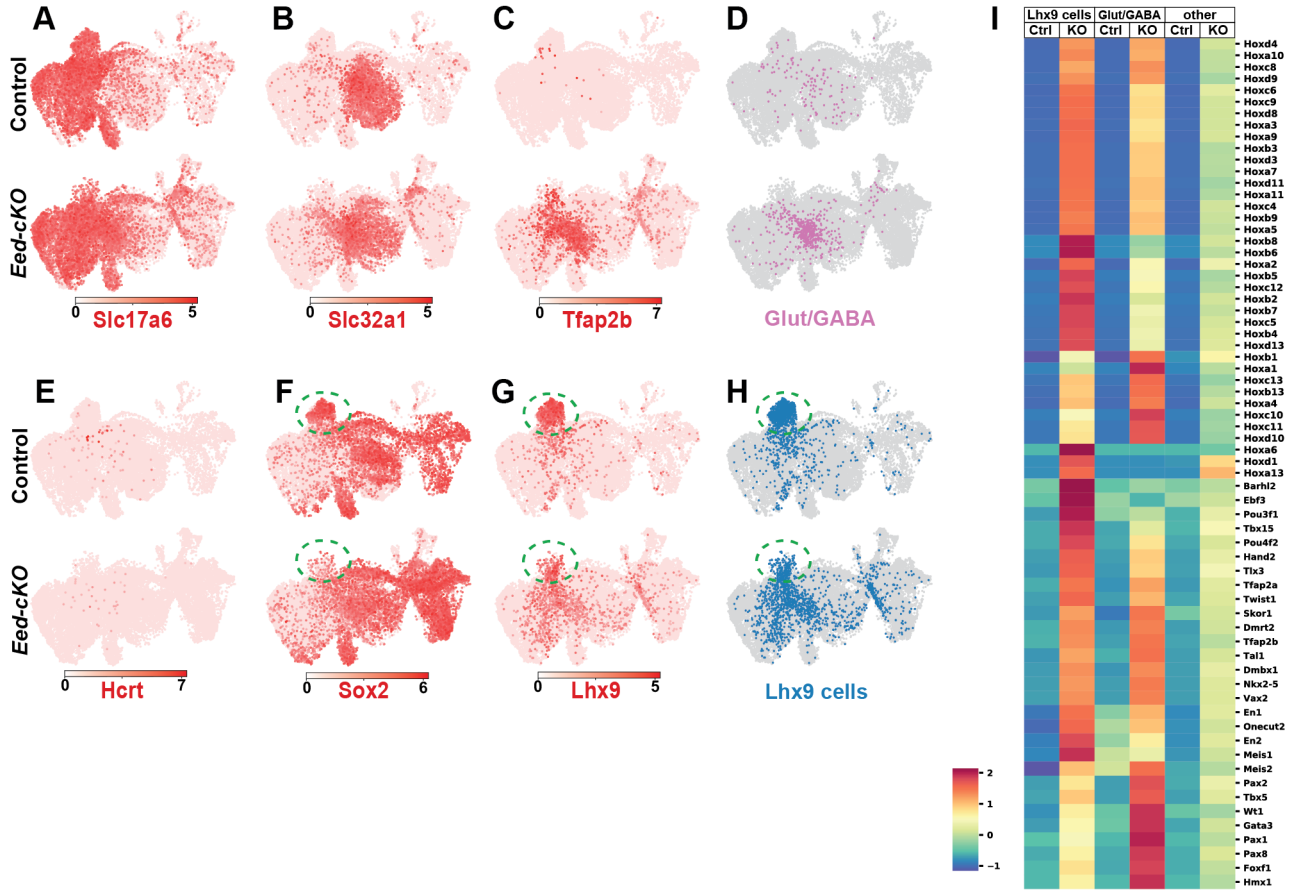

Supplemental Figure 1

Eed-cKO mutants lack H3K27me3 in the CNS

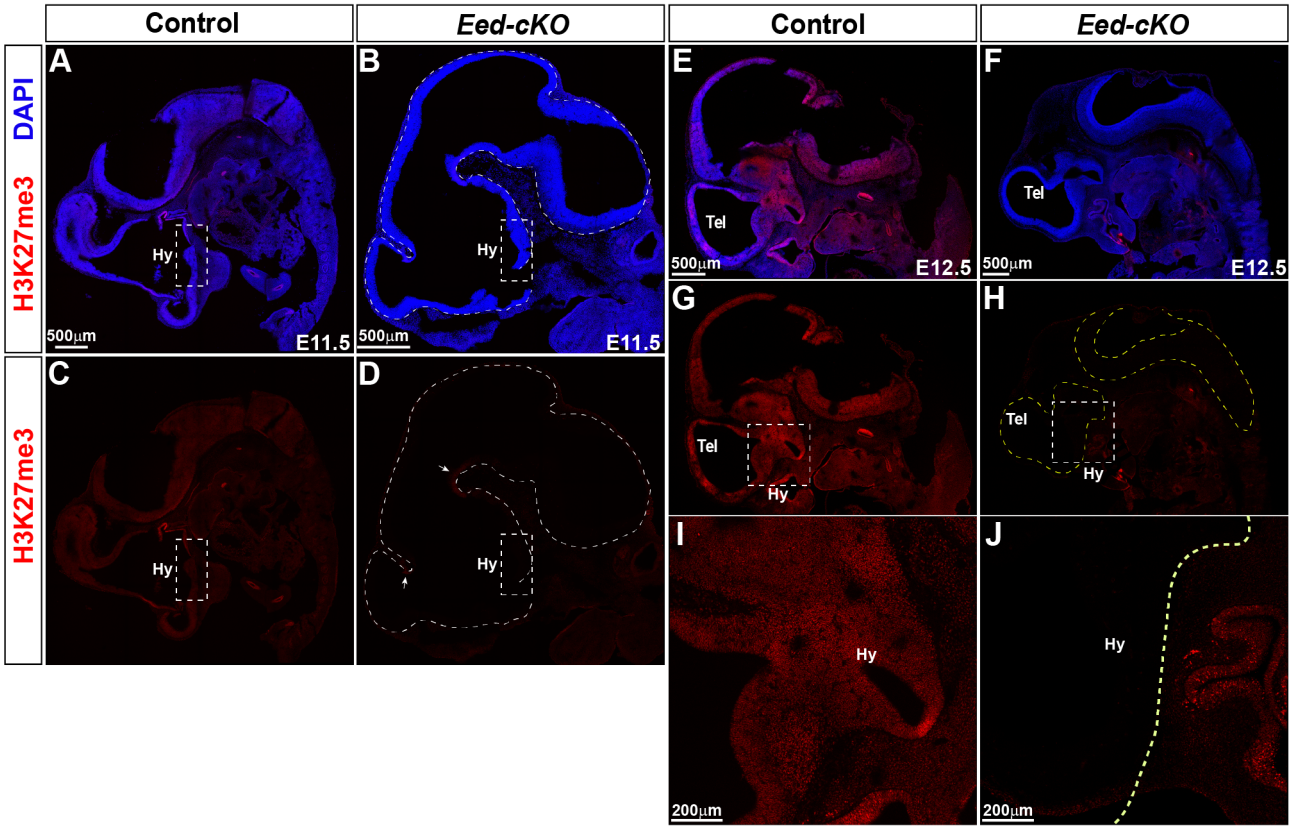

Supplemental Figure 2

Eed-cKO mutants display reduced proliferation

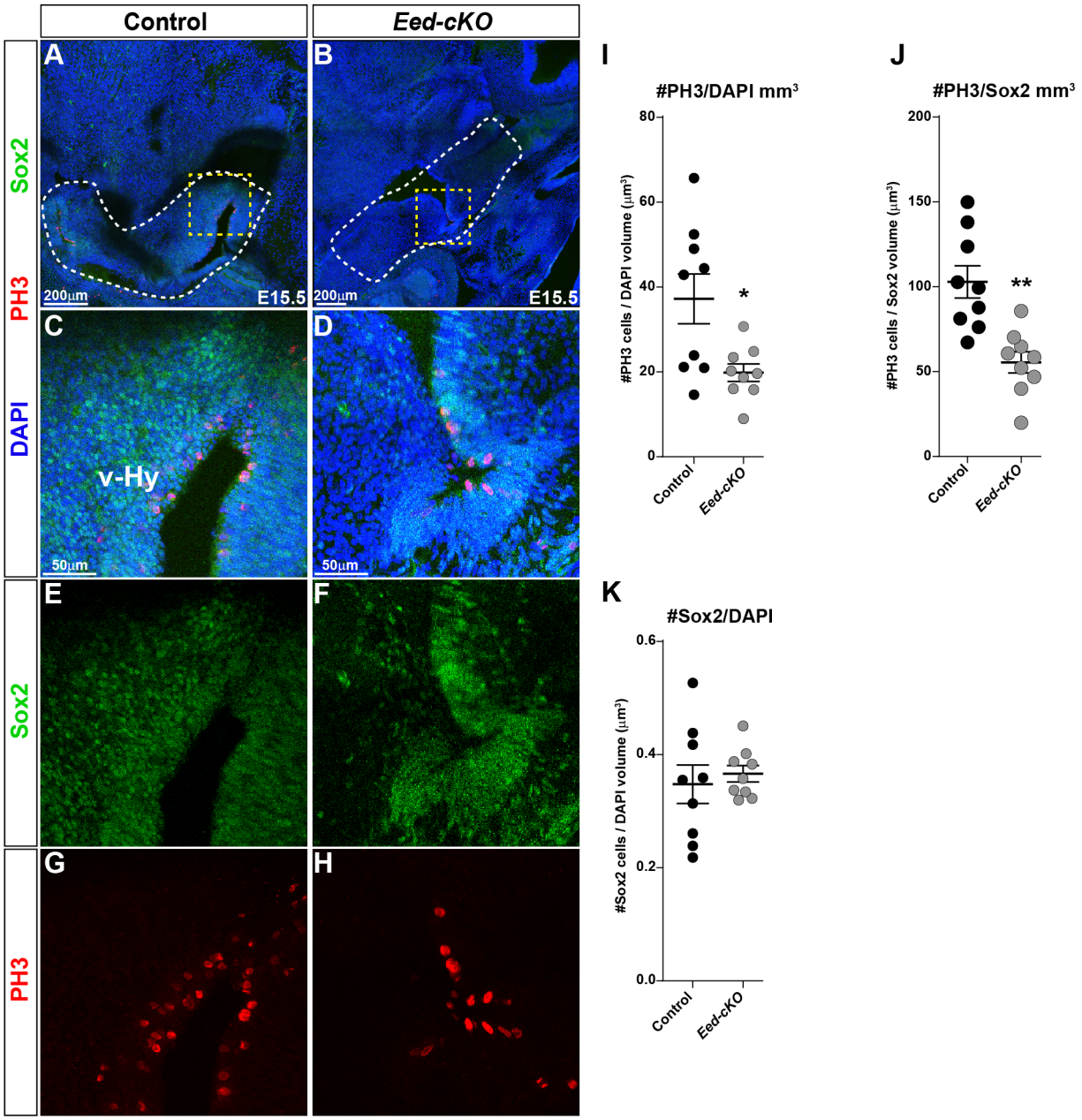

Supplemental Figure 3

Technical Filtering of scRNA-seq data

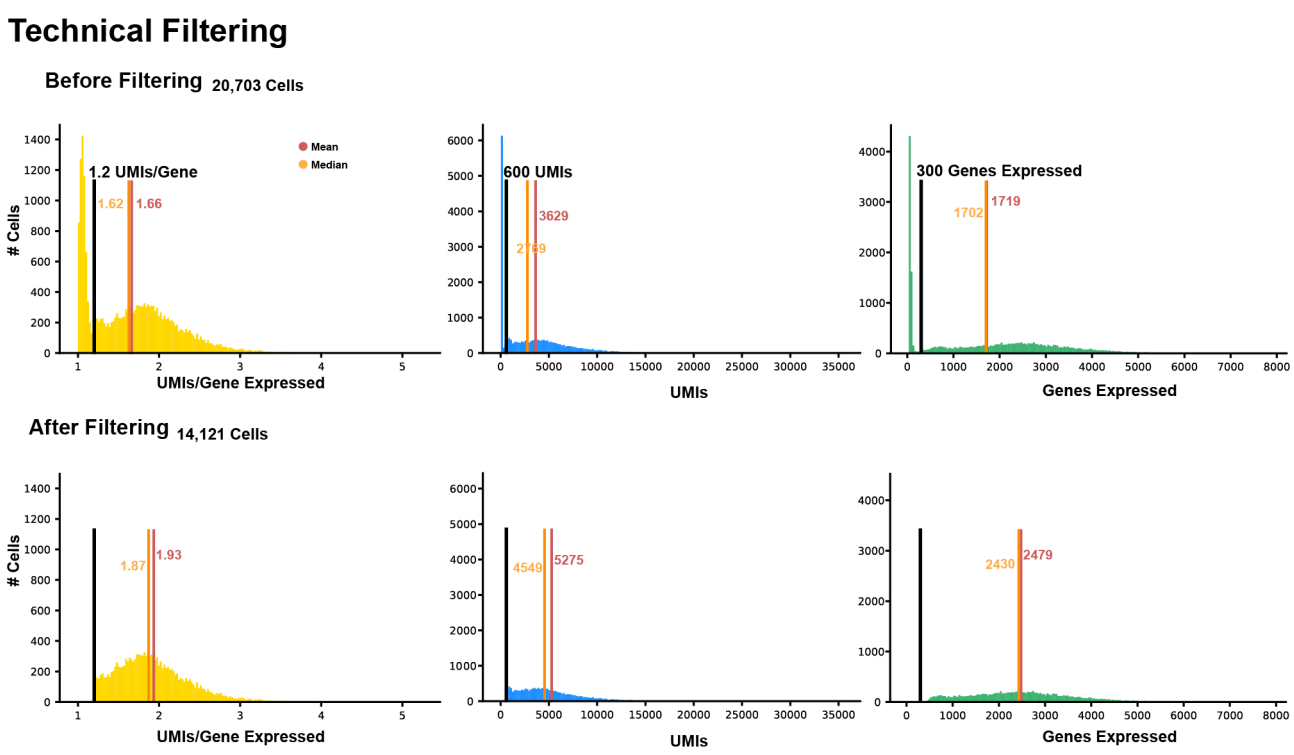

Supplemental Figure 4

GO Analysis in *Eed-cKO* Mutants

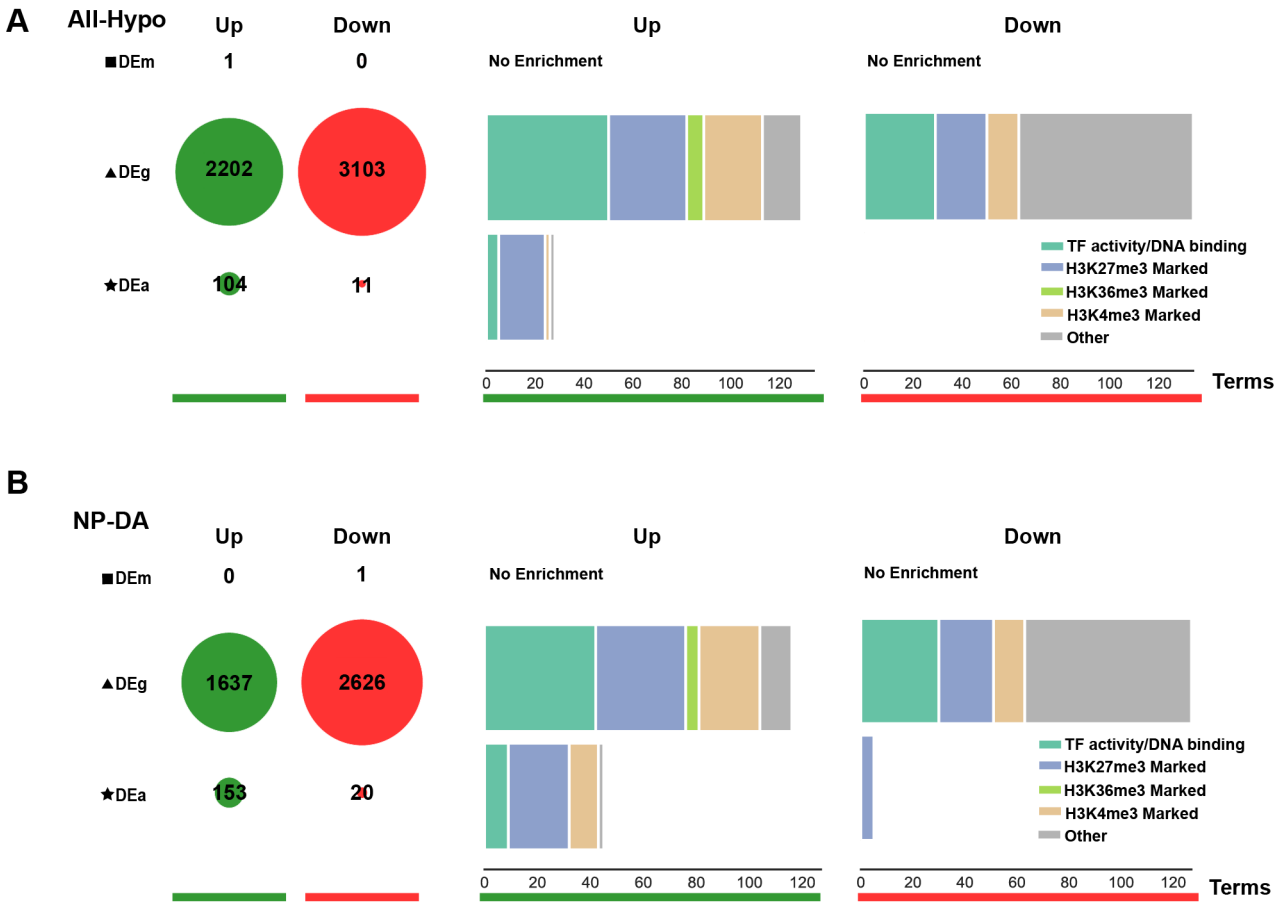

Supplemental Figure 5

Eed-cKO mutants display ectopic Pax2 expression

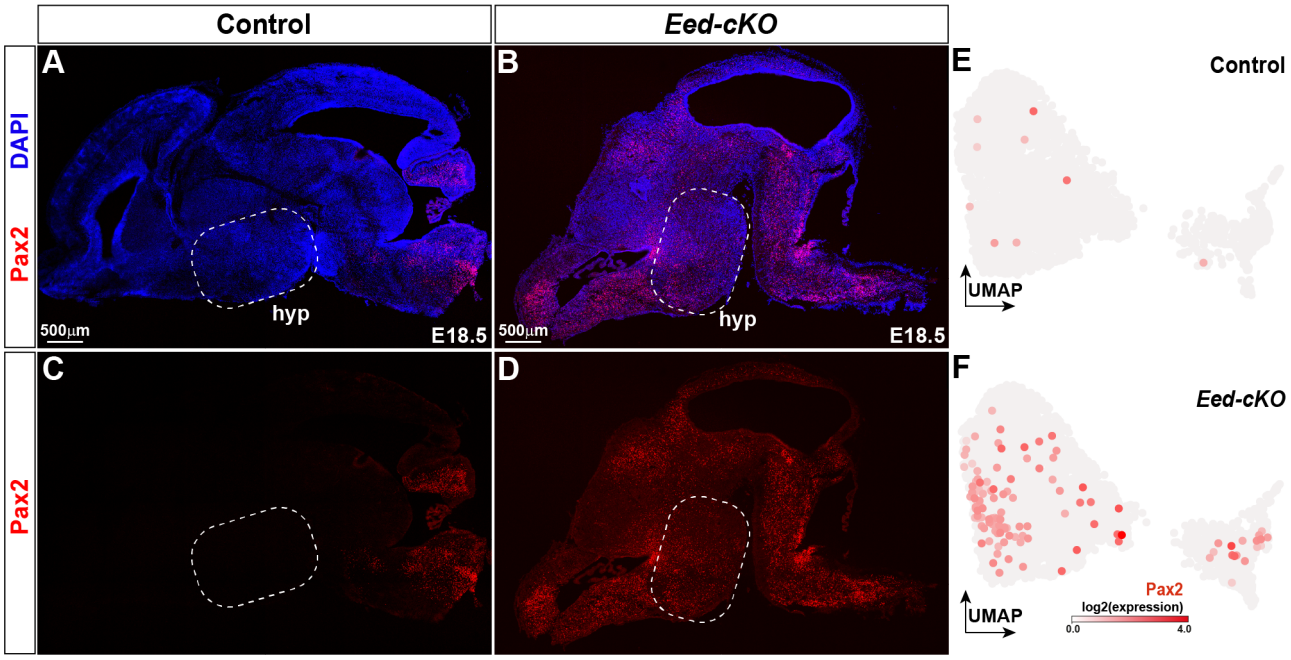

Supplemental Figure 6

Ectopic expression of posterior genes in *Eed-cKO*

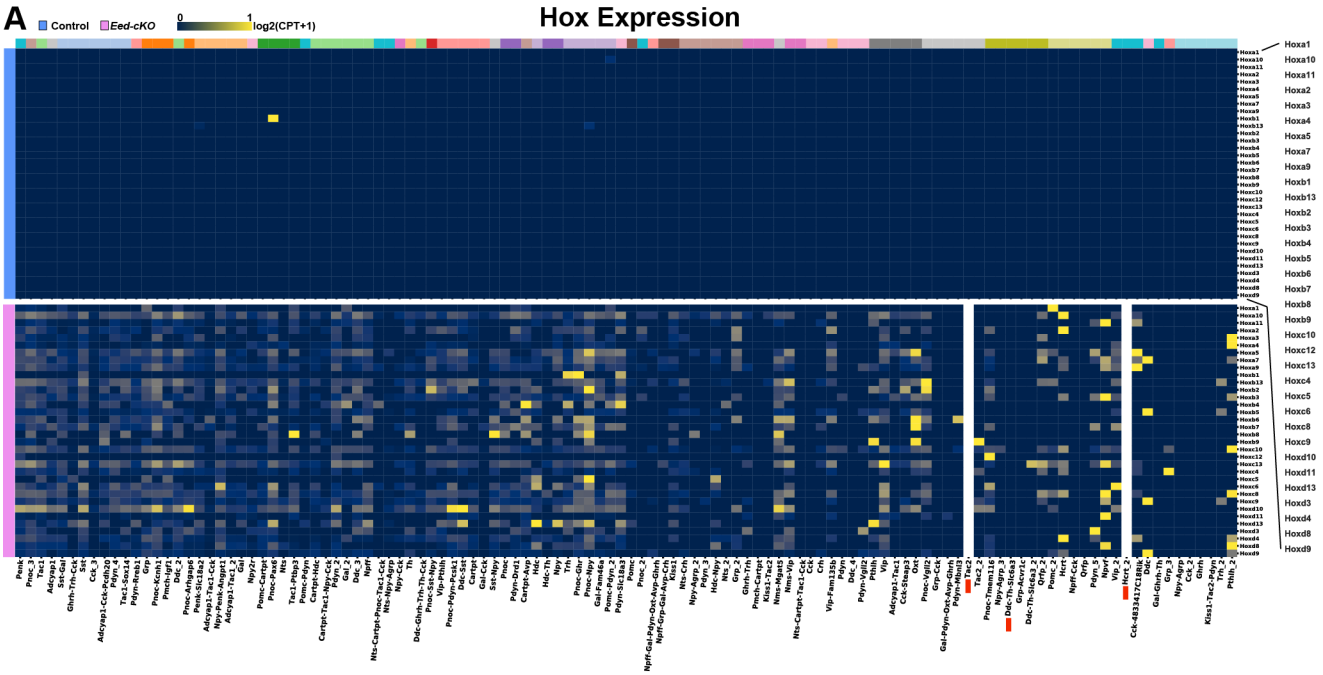

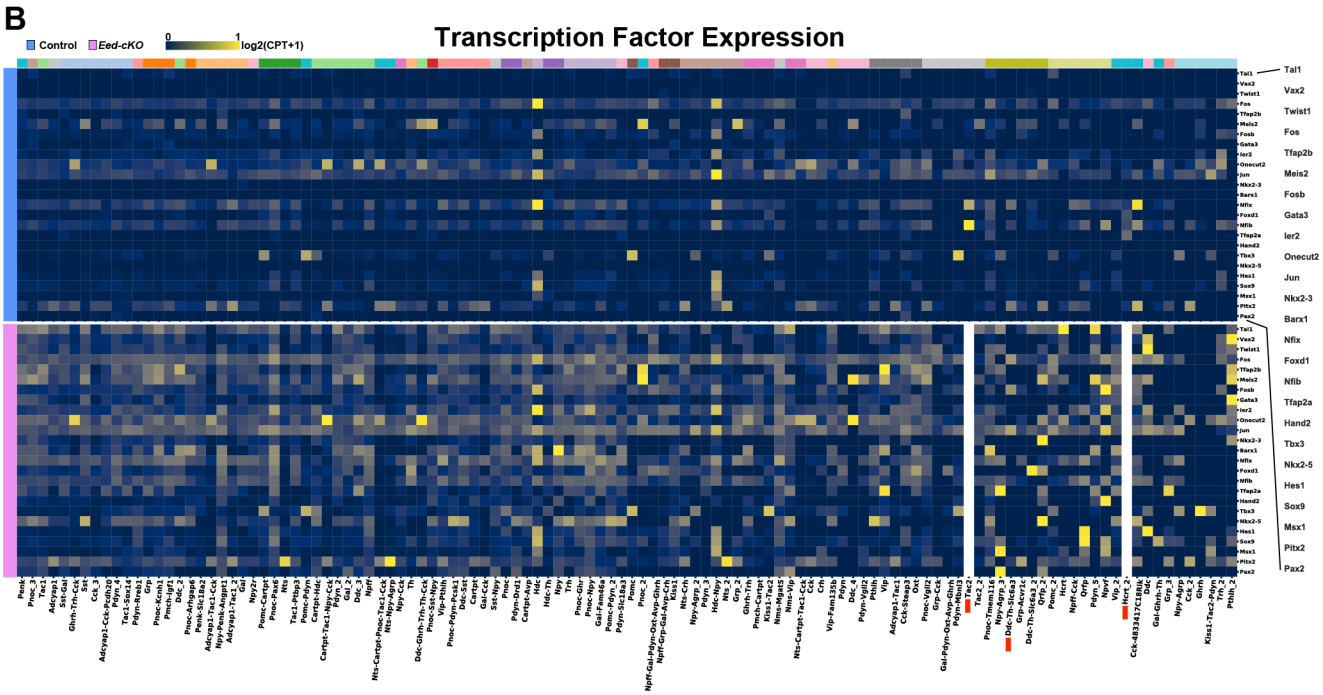

Supplemental Figure 7

Eed is not critical for Avp neurons

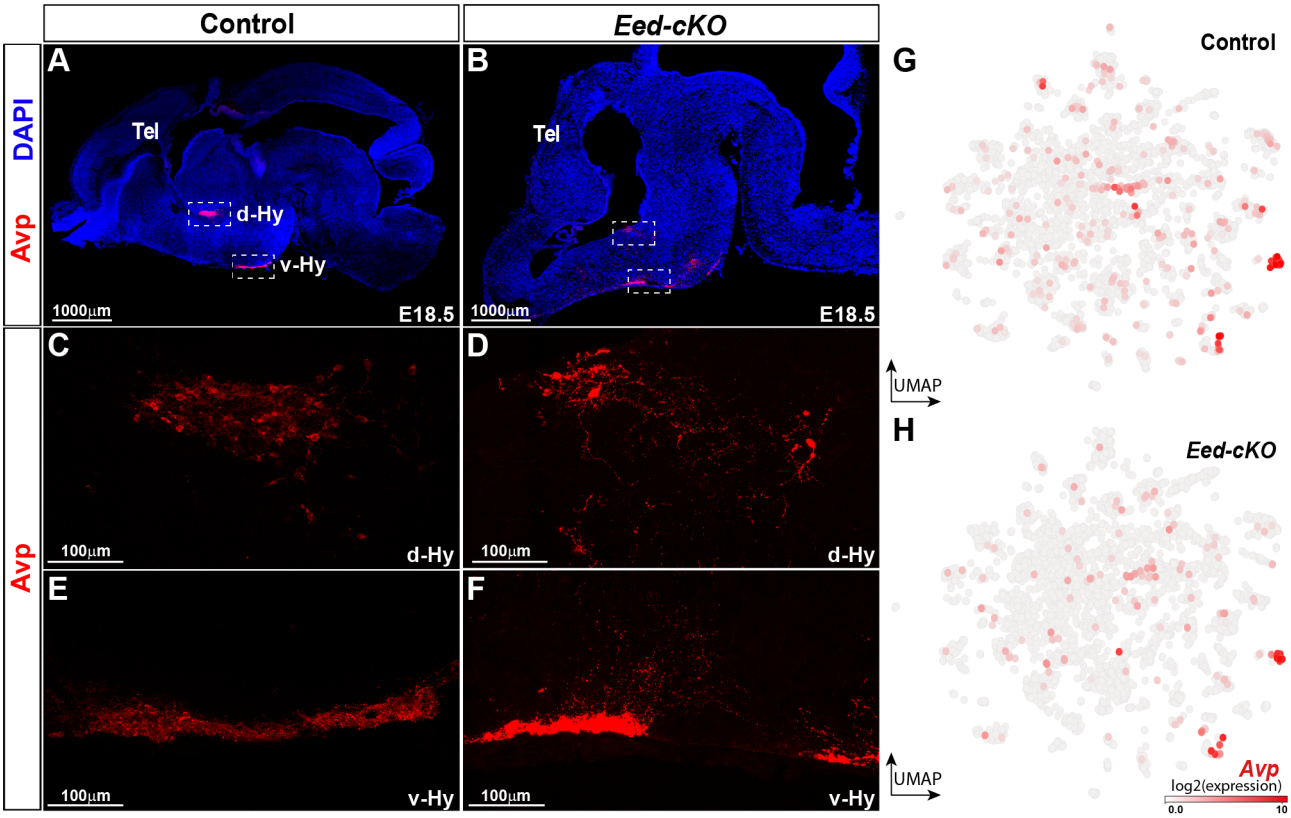

Supplemental Figure 8

Eed is not necessary for most NP-DA cell fates

Supplemental Figure 9

Eed is not necessary for most NP-DA cell fates

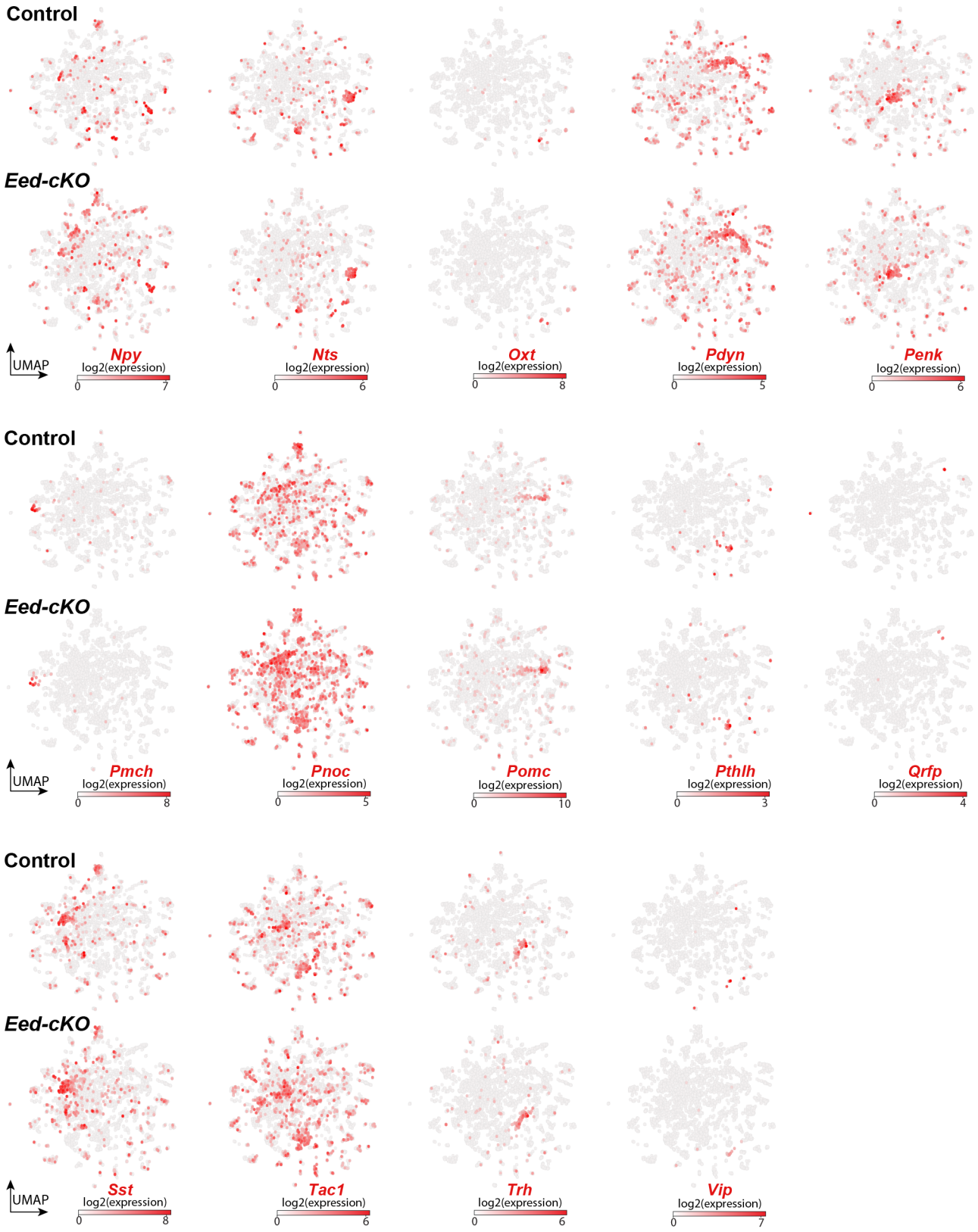

Supplemental Figure 10

Quality control and analysis of early time points

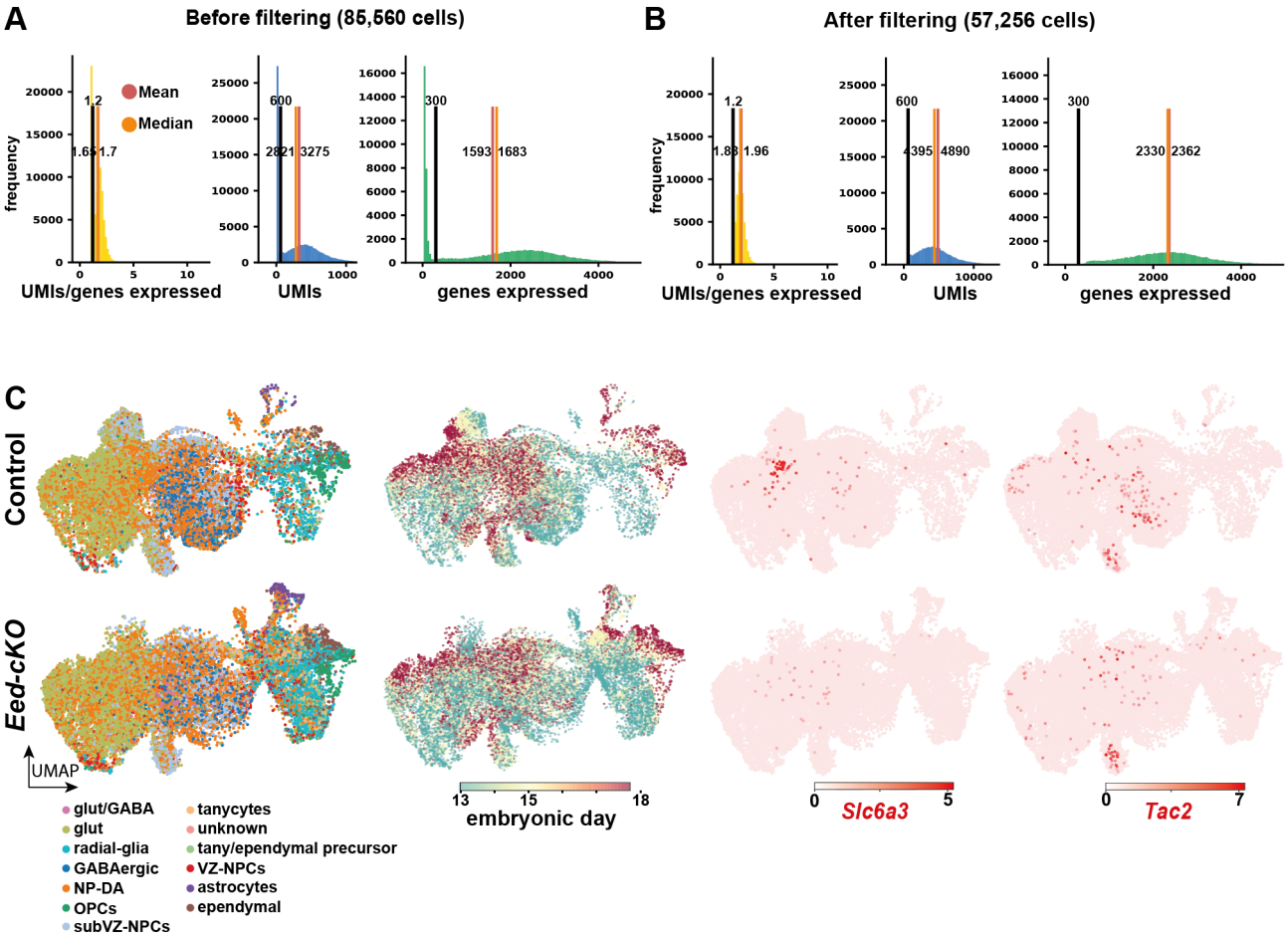

Table XIV. Gene lists used for UMAP analysis

List of genes used for PCA, prior to generating the All-Hypo and NP-DA UMAPs.
Note that the PCA was performed on WT cells alone, and then the learnt PCA transformation was applied to the KO cells.
The PCA spaces were then added together and the UMAP was performed on the PCA of both the WT and KO cells.

Understanding
All-Hypo analysis
In the case of the All-Hypo analysis, marker genes (**Broad Cell Type Markers**) differentiating different cell types (**Broad Cell Types**) were used to label cells.
When a cell expressed more than one marker, the marker with the higher expression was used to label the cell type.
The top 300 genes which had the highest normalised_mutual_information score
when considering the gene as 1 (on, having counts for that gene) or off (0) with the cell type labels were then selected for PCA and UMAP analysis (**PCA/UMAP All-Hypo Genes**).

NP-DA analysis
Neuropeptidergic-dopaminergic marker genes were compiled from the literature (**Granular NP-DA Gene Markers**).
The Pearson correlation coefficient of each gene measured with each marker was calculated in comparison to the log2(CPT+1) normalised data;
for each marker, the most correlated gene with that marker was added to a separate list and removed from a list of candidates, until 500 genes in total were selected.
From these 500 genes which had the highest correlation with atleast one marker, the top 123 genes with the highest Pearson correlation were selected for subsequent dimensionality reduction (**PCA/UMAP NP-DA Cells**).

CA/UMAP ALL-Hypo Gen	road Cell Type Marker	Broad Cell Types	PCA/UMAP NP-DA Genes	Granular NP-DA Gene Markers
Adhfe1	Gfap	Astrocyte	Efhc1	Nms
1500015O10Rik	Foxj1	Ependymal	Nms	Kiss1
Rftn2	Olig2	Oligodendrocyte Precursor	Rufy4	Vip
Catip	Olig1	Oligodendrocyte Precursor	Steap3	Pmch
Cdk5r2	Rax	Tanycyte	En1	Nts
Ccdc108	Slc32a1	GABAergic	Mgat5	Tac2
Resp18	Slc17a6	Glutamatergic	Kiss1	Ddc
Daw1			Kcnh1	Hcrt
Ramp1			Vip	Pomc
Tmem163			Vgll2	Cartpt
Prelp			Igf1	Pnoc
Nav1			Pmch	Npff
Kifap3			Parpbp	Sst
Atp1b1			Nts	Adcyap1
Cfap126			Nxph4	Grp
Atp1a2			Tac2	Gal
Kcnj10			Ddc	Qrfp
9330159F19Rik			Olfr1372-ps1	Hdc
Tspyl4			Slc25a35	Pdyn
Ccdc162			Lhx1	Oxt
Gja1			Lhx1os	Avp
Serinc1			4833417C18Rik	Ghrh
Fabp7			Hcrt	Crh
Chst3			Pomc	Penk
Gm17455			Fam150b	Tac1
Ank3			Nkx2-1	Npy
Rfx4			Ak7	Npvf
Timp3			Rreb1	Trh
Kif5a			Drd1	Pthlh
Egfr			Zfp369	Th
Cnrip1			Slc6a3	Agrp
Nsg2			Pcsk1	Cck
Gabrg2			Cartpt	
Sparc			Slc18a3	
Snap47			Pnoc	
Cfap52			Fam216b	
Chd3os			Pcdh20	
Cdk5r1			Ghr	
Dynll2			Angpt1	
Tmem100			Fam135b	
Hap1			1810041L15Rik	
Etv4			Odf3b	
Fzd2			Npff	
Gfap			Sst	
Mapt			Pcp4	
Sox9			Prss32	
Dnaic2			Grm4	
Slc9a3r1			Adcyap1	
Hn1			Tmem173	
Foxj1			Pcdhga8	
Vsnl1			Grp	
Myt1l			Gal	
Tspan13			Aldh1a1	
Hspa2			Pitx3	
Ppp1r36			Slc18a2	
Zfp36l1			Emx2	
Acot1			Qrfp	
Acot5			Mir7674	
Hecw1			Lhx2	
Tubb2a			Acvr1c	
Pxdc1			Pax6	
Nrn1			Hdc	
Map1b			Pdyn	
Rab3c			Oxt	
Gpx8			Avp	
Gng2			Ghrh	
Zcchc24			Crh	
Abhd4			Tmem212	
Mmp14			Tm4sf1	
Cmtm5			Tm4sf4	
Jph4			Npy2r	
Stmn4			Nhlh2	
Fam216b			Penk	
Rgcc			Ptbp3	
Ednrb			Dnali1	
Spry2			Abcb1b	
Sox21			Cacna2d1	
Sepp1			Asic3	
Slc1a3			En2	
Spef2			1700001C02Rik	
Ly6h			Fosl2	
Cdc42ep1			Slc10a4	
Sox10			Ambn	
Wnt7b			AW549542	
Mlc1			Tbx3	
Odf3b			Tmem116	
Dbx2			Calcr	
Emp2			Tfpi2	
2900011O08Rik			Tac1	
Lrrc74b			Npy	
Etv5			Npvf	
Hes1			Trh	
Itgb5			Lrrc23	
Igsf11			Pthlh	

Table S2. Differential expression in the All-Hypo and NP-DA cells.

This data shows the genes which were differentially expressed in Control (Ecad/+) when compared to Eed-cKO cells (Ecad/+;Sox2-Cre).
The method used to call differential expression was DESingle. All genes were tested that showed any expression across the cells (16, 504 in total), all of which are listed here.
The DE gene results from this analysis were used to show upregulation of HOX genes, and other regulators such as Pax2 and Tfap2b.
The DE results here also validated our observations from our clustering and UMAP visualisation that the neuropeptidergic and dopaminergic cell types were largely unaffected.

The structure for the sheets in this excel are as as follows:

DE Sheets Contains the direct output from DESingle, see here to understand the output (https://rdrr.io/bioc/DEsingle/man/DEsingle.html).
The most important columns are 'Type' and 'State'. For an explanation on the different types, please see below. This was extracted from the DESingle paper.
Genes are ordered according to their adjusted p-value.

DE_KOvWT_NP-DA -> Comparison of KO v WT cells - regardless of cluster - for just the neuropeptidergic/dopaminergic cells.

DE_KOvWT_ALL-Hypo - Comparison of KO v WT cells - regardless of cluster - for all of the cells which did not express Foxg1 and were not predicted as vasculature.
(i.e. initial cell type labels were not "Perivascular macrophages", "Microglia", "Vascular endothelial cells", "Vascular and leptomeningeal cells", "Pericytes", or "Choroid epithelial cells")

DE Types:

DEs Refers to 'different expression status'. It is the type of genes that show significant difference in the proportion of real zeros in the two groups, but do not have significant difference in the other cells.

DEa DEa is for 'DE abundance', which refers to genes that are significantly differentially expressed between the groups without significant difference in the proportion of real zeros.

DEg DEg or 'general differential expression' refers to genes that have significant difference in both the proportions of real zeros and the expression abundances between the two groups.

We found the **DEa** Instead of **DEs**, refers to 'differentially abundance of cells expressing gene between groups'.

DEm Instead of **DEa**, refers to gene being expressed at 'differential magnitude between groups'.

Deg Instead of **Deg,** refers to gene being generally differentially expressed (both in magnitude, and abundance).

This is denoted in the column 'Type_renamed' in the following sheets.

	theta_1	theta_2	mu_1	mu_2	size_1	size_2	prob_1	prob_2	otal_mean	otal_mean	foldChange	total_mea	total_mem	m_foldCha	chi2LR1	pvalue_1R2	pvalue_LR3	FDR_LR2	FDR_LR3	pvalue	value.adj.F	Remark	Type	State	pe_renamed
Hddc3	0.60602	0.9154	2.00209	1.72299	15389.4	10902.2	0.99987	0.99984	0.63255	0.10497	6.02626	0.78879	0.14576	5.41156	1438.92	0	1.6E-12	0	3.6E-12	0	0		DEg	up	DEg
Tal1	0.76686	0.98738	2.26952	2.37638	16187.4	12201.9	0.99986	0.99981	0.43745	0.0217	20.0986	0.5362	0.02999	17.8791	1420.13	0	0	0	0	0	0		DEg	[illegible]	DEg
Hoxc10	0.84687	1	2.18505	0	11890.5	1	0.99982	1	0.28942	0	inf	0.3346	0	inf	1187.23	0	0.16729	0	0.16988	0	0		DEs	up	DEa
Rps13	0.36259	0.15752	2.51257	3.22352	17853.8	11772.9	0.99986	0.99973	1.31065	2.21799	0.59092	1.60152	2.71574	0.58972	1004.3	0	0	0	0	0	0		DEg	down	DEg
Hoxb13	0.87212	0.9996	1.93549	1.59362	13186.7	15338.2	0.99985	0.9999	0.20595	0.00048	425.771	0.2475	0.00064	383.756	921.807	0	0	0	0	0	0		DEg	up	DEg
Hoxc13	0.88585	1	2.16672	0	11015.5	1	0.9998	1	0.20886	0	inf	0.24732	0	inf	871.263	0	0.21497	0	0.21811	0	0		DEs	up	DEa
Arl6ip1	0.35833	0.19575	2.59401	3.40321	13542.9	11384.2	0.99981	0.9997	1.34477	2.1801	0.61684	1.66449	2.73702	0.60814	836.895	0	0	0	0	0	0		DEg	down	DEg
Ccnd1	0.7705	0.95255	2.67958	2.41617	17190.3	14935.6	0.99984	0.99984	0.54019	0.10432	5.17817	0.61495	0.11464	5.36418	833.075	0	9.9E-06	0	1.3E-05	0	0		DEg	up	DEg
Hoxa10	0.89076	0.46398	1.99327	0.0006	14888.8	0.00024	0.99987	0.28478	0.18708	0.00016	1160.27	0.21775	0.00032	675.231	797.162	2E-10	0	2.3E-10	0	0	0		DEg	up	DEg
Vax2	0.89092	1	1.83326	0	13850.9	1	0.99987	1	0.15859	0	inf	0.19996	0	inf	787.156	0	0.21467	0	0.21783	0	0		DEs	up	DEa
Hoxa9	0.89546	1	2.02383	0	17152.6	1	0.99988	1	0.18726	0	inf	0.21158	0	inf	779.121	1.9E-12	0.24717	2.4E-12	0.25067	0	0		DEs	up	DEa
Xist	0.49023	0.73865	3.74609	4.13792	10186.3	11546.6	0.99963	0.99964	1.65796	0.93873	1.76617	1.90964	1.08143	1.76585	767.241	0	0	0	0	0	0		DEg	up	DEg
Ccnd2	0.7607	0.93518	2.91106	2.41294	15253	13254.5	0.99981	0.99982	0.62638	0.13351	4.69182	0.69661	0.1564	4.45397	735.643	0	1.8E-10	0	3.6E-10	0	0		DEg	up	DEg
Tfap2b	0.91009	0.99822	3.09179	5.43065	13135.3	13625.3	0.99976	0.9996	0.24333	0.00742	32.8074	0.27799	0.00967	28.7348	658.542	0	2.1E-06	0	2.9E-06	0	0		DEg	up	DEg
Hoxa7	0.91343	1	1.91785	0	18070.6	1	0.99989	1	0.14444	0	inf	0.16603	0	inf	630.255	4.8E-15	0.34028	6.4E-15	0.3449	0	0		DEs	up	DEa
Pisd-ps3	0.36091	0.59359	2.4696	2.20628	10918.9	10577.5	0.99977	0.99979	1.33478	0.69945	1.90833	1.5783	0.89665	1.76022	621.732	0	0	0	0	0	0		DEg	up	DEg
Mira	0.91384	1	1.83428	0	11340.5	1	0.99984	1	0.13156	0	inf	0.15805	0	inf	617.518	0	0.44856	0	0.45406	0	0		DEs	up	DEa
Bmi1	0.43355	0.65403	2.31382	1.94852	13281.8	16903.4	0.99983	0.99988	1.09109	0.51741	2.10874	1.31065	0.67414	1.94419	616.001	0	0	0	0	0	0		DEg	up	DEg
Hoxc8	0.91585	1	1.92342	0	14235	1	0.99986	1	0.13881	0	inf	0.16186	0	inf	612.764	3.4E-08	0.4311	3.7E-08	0.43663	0	0		DEs	up	DEa

	theta_1	theta_2	mu_1	mu_2	size_1	size_2	prob_1	prob_2	otal_mean	otal_mean	foldChang	total_m	total_m	m_foldCha	chi2LR1	pvalue_LR2	pvalue_LR3	FDR_LR2	FDR_LR3	pvalue	alue.adj.F	Remark	Type	State	pe_renamed
Hddc3	0.55563	0.9028	2.00674	1.71825	12206.3	11498.6	0.99984	0.99985	0.68332	0.11415	5.98602	0.89173	0.16702	5.33917	1160.87	0	1.1E-12	0	3.1E-12	0	0		DEg	up	DEg
Tal1	0.73935	0.98529	2.31028	2.36957	12241.1	11509.2	0.99981	0.99970	0.46831	0.02406	19.4637	0.60218	0.03485	17.2773	1114.16	0	6.9E-07	0	1.2E-06	0	0		DEg	up	DEg
Hoxc10	0.83025	1	2.19564	0	11336.1	1	0.99981	1	0.30502	0	inf	0.37272	0	inf	924.239	0	0.24687	0	0.25197	0	0		DEs	up	DEa
Rps13	0.31213	0.09985	2.49432	3.27769	12016.5	12282.9	0.99979	0.99973	1.3466	2.32959	0.57804	1.71577	2.95041	0.58154	899.066	0	0	0	0	0	0		DEg	down	DEg
Hoxb13	0.85746	0.99941	1.92285	1.59362	12710.6	18337.7	0.99985	0.99991	0.21121	0.0007	300.97	0.27409	0.00094	292.931	713.774	2E-09	8.7E-09	2.5E-09	1.8E-08	0	0		DEg	up	DEg
Xist	0.46063	0.74797	3.7654	4.18309	11710.8	10458.8	0.99968	0.9996	1.69752	0.86596	1.96026	2.03093	1.05427	1.92639	713.455	0	0	0	0	0	0		DEg	up	DEg
Hoxc13	0.87236	1	2.17119	0	15702.5	1	0.99986	1	0.22059	0	inf	0.27713	0	inf	682.77	0	0.3363	0	0.34247	0	0		DEs	up	DEa
Arl6ip1	0.29089	0.1386	2.58086	3.42812	12455.8	18717	0.99979	0.99982	1.43129	2.28749	0.6257	1.83012	2.95298	0.61975	663.243	0	0	0	0	0	0		DEg	down	DEg
Vax2	0.87424	1	1.82462	0	18825.7	1	0.9999	1	0.17216	0	inf	0.22946	0	inf	634.988	0	0.24086	0	0.24588	0	0		DEs	up	DEa
Ccnd1	0.78843	0.9661	2.45795	2.20793	12379.7	10396.9	0.9998	0.99979	0.41937	0.06058	6.92205	0.52003	0.07485	6.94728	615.873	0	6.5E-05	0	8.8E-05	0	0		DEg	up	DEg
Hoxa10	0.88205	0.99971	2.012	1.59362	14716.4	12229.8	0.99986	0.99987	0.1927	0.00023	823.783	0.23732	0.00047	507.277	601.651	0	0	0	0	0	0		DEg	up	DEg
Hoxa9	0.89202	1	2.03115	0	18077.5	1	0.99989	1	0.1823	0	inf	0.21932	0	inf	562.284	0	0.29871	0	0.30434	0	0		DEs	up	DEa
Pisd-ps3	0.29432	0.54666	2.47522	2.19397	12858.7	18432.4	0.99981	0.99988	1.40441	0.72959	1.92493	1.7467	0.99462	1.75615	521.252	0	0	0	0	0	0		DEg	up	DEg
Ccnd2	0.79874	0.95735	2.76898	2.19386	10974.6	14267.7	0.99975	0.99985	0.45563	0.07439	6.1252	0.5573	0.09357	5.95617	520.574	0	1.1E-08	0	2.3E-08	0	0		DEg	up	DEg
Twist1	0.89137	0.99803	1.87885	1.78233	12455.1	10437.8	0.99985	0.99983	0.15669	0.00257	60.8969	0.20411	0.00351	58.1706	490.404	0	7.1E-10	0	1.6E-09	0	0		DEg	up	DEg
Hoxd10	0.90637	1	2.07709	0	16795.9	1	0.99988	1	0.15492	0	inf	0.19447	0	inf	488.671	0	0.50971	0	0.51812	0	0		DEs	up	DEa
Fos	0.45826	0.69235	3.24062	2.87482	10466.2	18297.2	0.99969	0.99984	1.44168	0.72304	1.99392	1.75558	0.88444	1.98495	486.607	0	0	0	0	0	0		DEg	up	DEg
Bmi1	0.38685	0.62224	2.30497	1.93631	11119.2	13267.3	0.99979	0.99985	1.125	0.52725	2.13371	1.41329	0.73146	1.93214	483.846	0	0	0	0	0	0		DEg	up	DEg
Tfap2b	0.90472	0.99741	3.1081	5.24492	10091.6	12568.4	0.99969	0.99958	0.24468	0.01076	22.7389	0.29615	0.01357	21.828	471.706	0	1.3E-05	0	2E-05	0	0		DEg	up	DEg

Table S3. GO analysis of DE genes in the All-Hypo cells scRNA-seq data.

This data shows the GO terms that were enriched in each of our different types of DE genes which were differentially expressed between Ezh2 cKO and control.

Differentially expression was performed using **DESingle**; comparing ALL-Hypo cells between KO and WT.
Gene set enrichment was performed using **Enrichr**, as implimented in GSEAPY, against the '**GO_Molecular_Function_2018**' and '**ENCODE_Histone_Modifications_2015**' gene sets.

Interpretation
In essence, one can see via the 'Genes' column of each sheet which genes for that particular kind of DE gene set fell into different GO terms tested.
In the case of 'ENCODE_Histone_Modifications_2015' for the Gene_Set column, one can see genes marked by a particular histone mark in a particular sample on ENCODE.

For example, in the top row of the DEa_up sheet, we can see a signicant enrichment for genes that were marked with H3K27me3 in the mouse cerebellum.
(Adjusted P-value < 0.05, Term = H3K27me3 cerebellum mm9, first few Genes = HOTAIR;TCF21;HOXC13;MKI67;HOXC10;HOXA11;HOXA9;)

The structure for the sheets in this excel are as as follows:

DE Sheets

Each sheet contains statistics outputted from GSEAPY for performing GO Term enrichment performed on each kind of DE gene set.

Up' refers to genes which were upregulated in the KO compared to the WT.
Down' refers to the opposite.

DEa	Instead of **DEs from DESingle**, refers to 'differentially abundance of cells expressing gene between groups'.
DEm	Instead of **DEa from DESingle**, refers to gene being expressed at 'differential magnitude between groups'.
DEg	Refers to gene being generally differentially expressed (both in magnitude, and abundance).

	Adjusted P-value	Odds Ratio	Genes	Combined Score	P-value	Term
0	2.04125E-09	626.987	ENCODE_H	HOTAIR;TCF21;HOXC10;MKI67;HOXC11;HOXA9;CDH3;EOMES;	6.159158	27/1488	4.62106E-12	H3K27me3 cerebellum mm9
1	2.17771E-22	231.1335	ENCODE_H	HOTAIR;TCF21;RCSD1;HOXC10;CXCL16;HOXA11;HOXA9;HEY2;HOXA3;H	4.217687	62/2000	1.63928E-24	H3K27me3 ES-Bruce4 mm9
2	3.26657E-22	231.1335	ENCODE_H	HOTAIR;TCF21;RCSD1;HOXC10;CXCL16;HOXA11;HOXA9;HEY2;HOXA3;H	4.217687	62/2000	1.58571E-24	H3K27me3 ES-Bruce4 mm9
3	2.76727E-19	186.8862	ENCODE_H	LMOD1;HOXC13;RCSD1;HOXC10;HOXA11;HOXA9;HOXA3;HOXA2;HOXA	3.945578	58/2000	2.68667E-21	H3K27me3 testis mm9
4	1.26174E-15	139.595	ENCODE_H	HOTAIR;PRDM5;TCF21;RCSD1;HOXC10;HOXA9;CDH3;HEY2;HOXA3;HOX	3.605442	53/2000	1.53124E-17	H3K27me3 small intestine mm9
5	8.67343E-10	81.53469	ENCODE_H	HOTAIR;MYRF;FOXL2OS;TCF21;GATA4;HOXD13;HOXC13;MKI67;HOXD1	3.249061	40/1675	1.26312E-11	H3K27me3 kidney mm9
6	6.02588E-09	84.65438	ENCODE_H	FOXL2OS;FIGNL2;TCF21;HOXD13;RCSD1;HOXD11;TBX20;NKX2-5;PITX1;	3.680255	32/1183	1.02381E-10	H3K27me3 myocyte mm9
7	9.08296E-09	63.83047	ENCODE_H	HOTAIR;FIGNL2;TCF21;GATA4;ITPR3;HOXD13;HOXC13;HOXD11;HOXD1	2.857143	42/2000	1.98414E-10	H3K27me3 heart mm9
8	1.02183E-08	63.83047	ENCODE_H	COLEC12;MYRF;FOXL2OS;GATA4;HOXC13;CXCL16;HOXA9;TBX20;HEY2;	2.857143	42/2000	1.98414E-10	H3K27me3 spleen mm9
9	2.47041E-08	72.85307	ENCODE_H	FOXL2OS;FIGNL2;TCF21;HOXD11;HOXD10;NKX2-5;PITX1;OSR2;KCNH3;H	3.430844	32/1269	5.99613E-10	H3K27me3 C2C12 mm9
10	3.97233E-08	196.1891	GO_Molec	TCF21;GATA4;HOXD13;HOXC10;WT1;HAND2;HOXB3;HOXC4;HOXA1;HC	8.144103	17/284	3.4512E-11	transcriptional activator activity, RNA polymerase II transcription regulatory region sequence-specific binding (GO:0001228)
11	1.74668E-07	113.4783	ENCODE_H	OSR2;KCNH3;CDKN2A;TCF21;EVX1;HOXD13;RUNX2;HOXA11;HOXA9;PA	5.91541	17/391	4.66345E-09	H3K27me3 splenic B cell mm9
12	1.0029E-06	44.84706	ENCODE_H	HOTAIR;GYPA;LAMA4;PRDM5;LMOD1;SLC1A3;HOXD13;HOXC13;HOXC1	2.585034	38/2000	2.92106E-08	H3K27me3 liver mm9
13	2.96007E-06	40.74121	ENCODE_H	TMEM72;LMOD1;SLC1A3;GATA4;ITPR3;HOXC13;RCSD1;HOXD11;AK7;A	2.517007	37/2000	9.34002E-08	H3K27me3 NT2-D1 hg19
14	4.75565E-06	99.08474	GO_Molec	FOXD3;ESX1;PRDM5;GATA4;HOXC10;HAND2;TBX20;HOXB3;HOXC4;HO	5.323869	18/460	8.26351E-09	RNA polymerase II regulatory region sequence-specific DNA binding (GO:0000977)
15	1.01833E-05	36.16159	ENCODE_H	HOTAIR;TRADD;LAMA4;TCF21;GATA4;RCSD1;CDH3;EFEMP1;C1QTNF1;T	2.430749	36/2015	3.46035E-07	H3K27me3 H7 hg19
16	0.000142396	22.80538	ENCODE_H	TRADD;LAMA4;LMOD1;SLC1A3;TCF21;NOD1;GATA4;ITPR3;NID1;RCSD1;	1.87392	48/3485	5.1843E-06	H3K27me3 cardiac mesoderm hg19
17	0.000148002	26.70277	ENCODE_H	LAMA4;FOXL2OS;TMEM72;FIGNL2;GATA4;HOXD11;AK7;EFEMP1;C1QT	2.244898	33/2000	6.82532E-06	H3K4me1 limb mm9
18	0.000156224	26.70277	ENCODE_H	GYPA;LAMA4;LMOD1;FIGNL2;TCF21;NOD1;HOXD13;AK7;CXCL16;ERICH	2.244898	33/2000	6.82532E-06	H3K4me1 ES-Bruce4 mm9

Table S4. GO analysis of DE genes in the NP-DA cells scRNA-seq data.

This data shows the GO terms that were enriched in each of our different types of DE genes which were differentially expressed between Eed cKO and control.

Differentially expression was performed using **DESingle**; comparing NP-DA cells between KO and WT.
Gene set enrichment was performed using **Enrichr**, as implimented in GSEAPY, against the '**GO_Molecular_Function_2018**' and '**ENCODE_Histone_Modifications_2015**' gene sets.

Interpretation
In essence, one can see via the 'Genes' column of each sheet which genes for that particular kind of DE gene set fell into different GO terms tested.
In the case of 'ENCODE_Histone_Modifications_2015' for the Gene_Set column, one can see genes marked by a particular histone mark in a particular sample on ENCODE.

For example, in the top row of the DEa_up sheet, we can see a signicant enrichment for genes that were marked with H3K27me3 in the mouse cerebellum.
(Adjusted P-value < 0.05, Term = H3K27me3 cerebellum mm9, first few Genes = HOTAIR;HOXC13;MKI67;CCDC102A;HOXC10;HOXA11;HOXA9;HOXA3)

The structure for the sheets in this excel are as as follows:

DE Sheets

Each sheet contains statistics outputted from GSEAPY for performing GO Term enrichment performed on each kind of DE gene set.

Up' refers to genes which were upregulated in the KO compared to the WT.
Down' refers to the opposite.

DEa	Instead of **DEs from DESingle**, refers to 'differentially abundance of cells expressing gene between groups'.
DEm	Instead of **DEa from DESingle**, refers to gene being expressed at 'differential magnitude between groups'.
DEg	Refers to gene being generally differentially expressed (both in magnitude, and abundance).

	Adjusted P-value	mbined Sc	Gene_set	Genes	Odds Ratio	Overlap	P-value	Term
0	9.12108E-41	806.3529	ENCODE_H	HOTAIR;HOXC13;MKI67;CCDC102A;HOXC10;HOXA11;HOXA9;HOXA3;HOXA2;TSPO;HOXA7;PITX1;SOX	8.20996	61/1486	2.21385E-43	H3K27me3 cerebellum mm9
1	5.99988E-28	380.8477	ENCODE_H	HOTAIR;HOXC10;HOXA11;HOXA9;MKI67;HOXA3;HOXA2;HOXA7;PITX1;SOX7;HOXA5;HOXA4;FOXD3;1	5.6	56/2000	2.91957E-30	H3K27me3 ES-Bruce4 mm9
2	1.56663E-16	181.7853	ENCODE_H	HOTAIR;FOXC2;GATA4;HOXD13;HOXC13;HOXD11;HOXD10;HOXC10;HOXA11;HOXA9;HOXA3;HOXC5;	4.4	44/2000	1.14075E-18	H3K27me3 thymus mm9
3	3.76047E-14	145.7401	ENCODE_H	FOXC2;TMPRSS2;GATA4;HOXD13;HOXC13;HOXD11;HOXD10;HOXC10;HOXA11;ICAM1;HOXA9;TBX20;	4.1	41/2000	3.65094E-16	H3K27me3 testis mm9
4	3.69936E-11	105.1979	ENCODE_H	HOTAIR;GATA4;HOXD13;HOXD11;CCDC102A;HOXC10;HOXA9;TBX20;HOXA3;HOXC5;HOXA2;HOXC4;N	3.7	37/2000	4.48952E-13	H3K27me3 small intestine mm9
5	9.52334E-10	313.4703	GO_Molec	FOXC2;GATA4;HOXD13;HOXC10;HAND2;E2F2;HOXB3;HOXC4;HOXB2;HOXD4;HOXD3;HOXA7;NKX2-5;	11.26761	16/284	8.27397E-13	transcriptional activator activity, RNA polymerase II transcription regulatory region sequence-specific binding (GO:0001228)
6	5.95685E-09	188.3485	ENCODE_H	FOXC2;CDKN2A;FST;PAX3;EVX1;HOXD13;HOXA11;HOXA9;PAX9;HOXB2;HOXA7;HOXC9;HOXC8;HOXD	8.184143	16/391	1.01209E-10	H3K27me3 splenic B cell mm9
7	6.27328E-09	101.6098	ENCODE_H	TMPRSS2;HOXD13;HOXD11;ICAM1;ALOX8;TBX20;RPRML;NKX2-5;PITX1;SOX7;CD70;EVX1;VAX2;HOXI	4.395604	26/1183	9.13584E-11	H3K27me3 myocyte mm9
8	1.44103E-08	72.58978	ENCODE_H	HOTAIR;WDR63;GATA4;HOXD13;HOXC13;HOXD11;HOXD10;HOXC10;HOXA11;ALOX8;TBX20;HOXA2;H	3.3	33/2000	2.79812E-10	H3K27me3 heart mm9
9	1.91166E-08	88.49633	ENCODE_H	HOXD11;HOXD10;ICAM1;ALOX8;RPRML;NKX2-5;PITX1;SOX7;CD70;EVX1;HOXB9;SST;TLX1;FEV;PAX9;I	4.097715	26/1269	4.17595E-10	H3K27me3 C2C12 mm9
10	6.96836E-08	168.777	GO_Molec	FOXD3;ESX1;GATA4;HOXC10;HAND2;TBX20;E2F2;HOXB3;HOXC4;HOXD4;HOXD3;HOXA7;NKX2-5;HOX	7.391304	17/460	1.21084E-10	RNA polymerase II regulatory region sequence-specific DNA binding (GO:0000977)
11	3.01472E-07	62.62983	ENCODE_H	HOTAIR;FOXC2;GATA4;HOXD13;HOXC13;MKI67;HOXD11;CCDC102A;HOXA11;TBX20;NKX2-5;PITX1;S(	3.343284	28/1675	7.31727E-09	H3K27me3 kidney mm9
12	2.00032E-06	208.748	GO_Molec	FOXD3;HAND2;ESX1;TBX20;E2F2;GATA4;HOXD4;HOXD3;HOXD9;HOXD8;HOXC10	10.94527	11/201	5.21369E-09	RNA polymerase II regulatory region DNA binding (GO:0001012)
13	3.20652E-06	47.19301	ENCODE_H	TMPRSS2;GATA4;HOXC13;CCDC102A;HOXA9;TBX20;HOXC5;HOXC4;HOXA7;NKX2-5;HOXC6;FOXD3;FS	2.9	29/2000	8.56109E-08	H3K27me3 spleen mm9
14	6.85798E-05	114.8943	GO_Molec	FOXD3;HAND2;ESX1;TBX20;E2F2;GATA4;HOXD4;HOXD3;HOXD9;HOXD8;HOXC10	7.534247	11/292	2.38331E-07	transcription regulatory region sequence-specific DNA binding (GO:0000976)
15	0.000828593	22.93005	ENCODE_H	HOXD13;HOXC13;HOXD10;HOXA11;BC107364;HOXA9;HOXA3;APOE;HOXA7;NKX2-5;PITX1;SOX7;HOX	2.156722	30/2782	2.41338E-05	H3K9me3 G1E-ER4 mm9
16	0.001191238	24.45321	ENCODE_H	FOXD3;FOXC2;TRPC6;ESX1;FZD6;KLK4;HOXD11;VAX2;HOXA9;CXCL12;SST;HOXC5;HOXC4;HOXB2;APC	2.4	24/2000	3.75876E-05	H3K27me3 mononuclear cell hg19
17	0.001371589	19.46098	ENCODE_H	FOXC2;TMPRSS2;KLK4;GATA4;HOXA11;ICAM1;TBX20;HOXA2;TSPO;RPRML;NKX2-5;SOX7;HOXA5;FOX	1.95122	34/3485	4.66074E-05	H3K27me3 cardiac mesoderm hg19
18	0.003352727	20.57091	ENCODE_H	HOTAIR;PRRX1;CD70;ESX1;FZD6;IGF2;ADAM33;PAX3;KLK4;EVX1;GATA4;SST;TLX1;HAND2;TBX20;PAX	2.282878	23/2015	0.000122065	H3K27me3 H7 hg19

Table S5 | DE genes in NPOR UMAP clusters

This data shows the genes which were differentially expressed in our NPOR clusters.
The method used to call differential expression was independent t-tests with the Bonferroni method to correct for multiple hypothesis testing.
Each gene indicated of the 16, 511 which had counts were tested, provided they had expression in the cluster.
All genes tested for each cluster are shown in the relevant sheet.
These tests were performed using the scipy.stats.ttest_ind function with scipy version 1.4.1.
Genes were considered up- or down- regulated if the adjusted p-value was <.05 and the t-statistic was greater than 0 or less than 0, respectively.
The DE gene results from all cells was used to annotate the cell types in the paper.

The structure for the sheets in this excel are as as follows:

Summary DE Sheets	Contains summaries of the DE results across all of the clusters.
deGenesByCluster_all ->	Using all cells - regardless of treatment - up and down regulated genes for each cluster are summarised. This was performed by comparing cells within the cluster to the remaining cells (one-versus-rest comparison).
deGenesByCluster_wt ->	The same as deGenesByCluster_all, except performed on the wild-type (wt, 'control' in paper) cells alone.
deGenesByCluster_ko ->	The same as deGenesByCluster_all, except performed on the knock-out (ko, 'Eed-cKO' in paper) alone.
deGenesByCluster_KOvWT ->	Contains the up- and down- regulated genes when comparing KO cells to WT cells within clusters. Up- refers to genes upregulated in the KO cells and down- refesr to genes downregulated in the KO. These results were not discussed within the paper, since we observed whether genes were called DE largely depends on the size of the cluster. Instead, we used DESingle to compare KO v WT cells - regardless of cluster. The results from this comparison are in a different supplementary.
Cluster DE Sheets	Contains the full DE results for each cluster, including all relevant statistics. Note that {cluster_name}_prop_expr_in column refers to percentage of cells which express the gene within the cluster, and {cluster_name}_prop_expr_out refers to percentage of cells which express the gene in the rest of the cells.
deGenesByCluster_all_stats ->	Contains results for the OVR comparison for the particular cluster NAME. Includes all relevant statisitcs (such as p-values). Summarised across cluster in deGenesByCluster_all.
deGenesByCluster_wt_stats ->	Same as deGenesByCluster_all_stats, except just for WT cells. Results across clusters sumarrised in deGenesByCluster_wt.
deGenesByCluster_ko_stats ->	Same as deGenesByCluster_all_stats, except just for KO cells. Results across clusters sumarised in deGenesByCluster_ko.
deGenesByCluster_KOvWT_stats ->	Contains the results from comparing KO to WT cells within the particular cluster. Summarised across each cluster in deGenesByCluster_KOvWT.

	Adcyap1_up	Adcyap1_down	Adcyap1-Cck-Pcdh20_up	Adcyap1-Cck-Pcdh20_down	Adcyap1-Tac1	Adcyap1-Tac1_down
0	Adcyap1	Gad1	Pcdh20		Tac1	
1	Lmx1a	Lhx1os	Pla2g3		2210039B01Rik	
2	Barhl1	Isl1	Kcnj15		Adcyap1	
3	Barhl2	Slc32a1	Gm15408		4930525D18Rik	
4	Calb2	Efna5	Stfa2l1		Gm38426	
5	Pitx2		Gm19689		Frs3os	
6	Nr4a2		Gpr17		Gbp8	
7	Slc17a6		Sox10		Wfdc3	
8	Irx5		Alcam		Foxa1	
9	Ptpre		Fzd10		Upk1b	
10	Gm5105		Pcdh19		Gm16793	
11	Cacna2d1		Gm4926		Sds	
12	Nrn1		4833422C13Rik		Cutal	
13	Gsc		Gabrb2		Fam19a3	
14	2900041M22Rik		Gabra3		Sprtn	
15	Cpne8				Nlrc4	
16	Fgd5				Gm2897	
17	Fstl5				Zp1	
18	Syt4				Npsr1	
19	Prkcb				Tspear	
20	Vsnl1				Prss16	
21	Hrct1				Dnajc16	
22	Cdh23				Il23a	
23	Fxyd7				Abca6	
24	Dmrta2				Mab21l1	
25	Mos				Birc3	
26	Bdnf				Apoc3	
27	Foxa1				C1ql3	
28	Gabrr1				Uckl1os	
29	Tmeff2				D630039A03Rik	
30	Bfsp2				Ces1d	
31	Pbx3				Itgae	
32	Nhlrc3				Cacna2d1	
33	Sv2b				Pawr	
34	Foxo3				Lmx1a	
35	Tpbg				Sdpr	
36	Chl1				Gm6578	
37	Lppr4				Csf2rb	
38	Spryd7				Gm29684	
39	1700008O03Rik				Rhoh	
40	1810041L15Rik				Neurl3	
41	Cbln1				Myof	
42	Scg2				Khk	
43	Bcl11b				Rab25	
44	Ace2				Rbm47	
45	Cblc				1700108F19Rik	
46	Ppp3ca					
47	Rbfox1					
48	Apoh					
49	Hmgcs1					
50	Cdc42bpb					
51	Slc1a1					
52	Sybu					
53	Pknox2					
54	Nrxn1					
55	Cbln2					
56						
57						
58						
59						
60						
61						
62						
63						
64						

Table S6. Temporal onset of NP-DA genes

E11.5	E13.5	E15.5	E18.5	P4	Transmitters	Ref	DE analysis
					Adcyap1	ABA	
					Pomc	ABA	Up DEg
					Ddc	ABA	Down DEg
					Pmch	ABA	Down DEa
					Sst	ABA, Diaz et al.	Up DEa
					Th	ABA, Diaz et al.	Down DEg
					Trh	ABA, Diaz et al.	
					Tac1	ABA	Up DEg
					Avp	ABA	Down DEa
					Cartpt	ABA	Up DEg
					Crh	ABA, Diaz et al.	Down DEg
					Kiss1	Knoll et al.	
					Npvf	ABA	
					Npy	ABA	Up DEg
					Pdyn	ABA	
					Pnoc	ABA	Up DEg
					Grp	ABA	Down DEg
					Agrp	ABA	
					Cck	ABA	Up DEg
					Gal	ABA	Down DEg
					Ghrh	ABA, Diaz et al.	Down DEg
					Hcrt	ABA	Down DEg
					Nts	ABA	
					Oxt	ABA	
					Penk	ABA	
					Hdc	ABA	Up DEg
					Pthlh	ABA	
					Tac2	ABA	
					Vip	ABA	
ND	ND	ND	ND	ND	Nms		
ND	ND	ND	ND	ND	Npff		
ND	ND	ND	ND	ND	Prlh		
ND	ND	ND	ND	ND	Qrfp		
ND	ND	ND	ND	ND	Galp		

Table S7: Source Data for Figure S2

selection along the tissue rim of a 400um width (segmented line)
selection is straightened
2nd selection of 1000um in length of straightened tissue
final analyzed tissue selection 400x1000 um

In Java, the integer is also 32 bits, but ranges from -2,147,483,648 to +2,147,483,647.
64 bit -9 223 372 036 854 775 808 +9 223 372 036 854 775 807
test of volumetrics- system max-out (3D viewer)
C1-F655E4 S34a=fl-+ ++=e15.5=pH3 rat RedX, sox2 rbt 1;300 FITC, DAPI=sagittal=Hy -1

		DAPI-all	volume	1834281980.00
maxed out value for JAVA-based 32-bit integer				
	2.15E+09			
maxed out value for JAVA-based 64-bit integer		DAPI500-1	volume	820132220.00
	9.22337E+18	DAPI500-2	volume	1014072960.00
thresholding methods:			sum	1834205180.00
DAPI: Huang				
Sox2: Moments		DAPI-450	volume	741078660.00
		DAPI-350	volume	730276290.00
		DAPI-200	volume	362773312.00
			sum	1834128262.00

Relevant information for labelling the cell types for the cells in the dataset.

Understanding

broad_markers

Contains the marker genes used for the labelling of the cells as described in the methods.

The logical notation:

'|' for 'or', which in the pos_expr column means that cells expressing any of the genes listed are considered in that category when labelled, while in the neg_expr column cells expressing any genes separated by '|' would not be considerd in that category.

',' is for 'and', meaning any cells expressing all genes listed in the positive column are considered in that category, while cells expressing all genes separated with ',' would not be considered in that category.

Using ',' and '/' in combination, the '/' groups the genes into sets; so if we have 'A,B|B,C' in pos_expr column, then cells which express (A AND B) OR (B AND C), would be considered in that category.

In the neg_expr column, any cell matching this criteria would not be grouped in that category.

Recall from the methods that in this table, the cell labels are listed from labelled first to labelled last, such that latter cell labellings override previous cell labellings.

Cells not matching any criteria at any point are labelled 'unknown'. These were few and far between, and most were successfully labelled with the logistic regression afterward.

confusion_matrix

The confusion matrix from the logistic regression classification of a random training set of 20% of binary labelled cells.

The rows are the actual labels of the cells for the training set.

The columns are the predicted labels.

The elements in the matrix contain the count of cells which had the indicated actual/predicted labels indicated by the rows and the columns.

	pos_expr	neg_expr
other-neuron	Adcyap1/Agrp/Avp/Cartpt/Cck/Crh/	
radial-glia	Fabp7	
ependymal	Foxj1/Mia/Meig1	
glutamatergic	Slc17a6	Slc32a1
GABAergic	Slc32a1	Slc17a6
gluta/GABA	Slc17a6,Slc32a1	
subVZ-NPCs	Sox2,Adcyap1/Sox2,Agrp/Sox2,Avp/	Zfp36l1/Ccnd1
subVZ-NPCs	Sox2,Slc17a6/Sox2,Slc32a1	Zfp36l1/Ccnd1
VZ-NPCs	Hes5,Adcyap1/Hes5,Agrp/Hes5,Avp/	Zfp36l1/Ccnd1
VZ-NPCs	Hes5,Slc17a6/Hes5,Slc32a1	Zfp36l1/Ccnd1
OPCs	Olig1	Mia/Meig1
tanycytes	Rax	
tanycytes/ependymal precursors	Rax,Hes5	
astrocytes	Igf2,Foxc1,Col4a2	

	GABAergic	OPCs	VZ-NPCs	astrocytes	ependymal	gluta/GABA	glutamaterg	other-neuro	radial-glia	subVZ-NPCs	tanycytes	ependymal	unknown
GABAergic	866	3	4	0	2	4	9	8	1	31	3	0	1
OPCs	1	208	0	0	2	0	1	0	5	0	0	0	0
VZ-NPCs	9	2	86	0	5	0	17	23	30	9	0	1	2
astrocytes	0	1	0	87	1	0	1	7	0	1	0	0	0
ependymal	6	5	2	0	245	0	17	11	16	9	2	1	0
gluta/GABA	22	0	3	0	0	86	21	0	0	4	0	0	3
lutamaterg	1	1	8	0	1	2	2175	8	11	43	0	0	1
ther-neuro	79	4	10	4	2	0	140	1916	30	43	5	1	3
radial-glia	4	12	19	1	19	0	1	21	689	9	2	3	0
subVZ-NPCs	18	1	2	0	6	1	34	52	9	695	2	0	0
tanycytes	0	0	0	0	2	0	4	3	0	3	128	2	0
ependymal	0	0	0	0	0	0	0	0	6	1	1	81	1
unknown	0	0	0	0	0	0	0	0	0	0	0	0	0

Table S9. Differential gene expression changes in specific cells

	tvals	pvals	pvals_adj	logFC
Hoxa9	33.33638	2.53E-18	1.21E-15	30.75007
Hoxa5	32.75009	3.52E-18	1.38E-15	29.38509
Meis2	32.31477	1.19E-25	1.51E-21	3.673903
Tal1	31.06243	5.58E-18	2.09E-15	7.476678
Hoxb7	29.79492	2.06E-17	6.36E-15	29.00135
Hoxc8	29.17854	3.03E-17	8.92E-15	28.77946
Bmi1	26.31524	1.72E-25	1.51E-21	2.119488
Hddc3	26.14458	2.49E-24	1.46E-20	3.086747
Meis1	25.84651	2.53E-22	4.47E-19	3.487031
Hoxa10	25.15477	4.59E-16	9.31E-14	10.48788
Hoxc9	24.22229	9.54E-16	1.81E-13	29.19356
Onecut2	24.21285	2.32E-19	1.57E-16	2.561906
Tfap2b	23.99061	4.49E-19	2.93E-16	4.887017
Hoxc13	23.76941	1.35E-15	2.47E-13	29.3826
Vax2	23.39516	1.28E-15	2.39E-13	7.895493
Crabp1	23.01755	3.87E-16	8.03E-14	5.718598
Tpt1	22.91051	9.98E-24	4.4E-20	1.372062

Table S10. Differential gene expression in subsets of cells

	tvals	pvals	pvals_adj	logFC
Lhx9	117.5029	1.17E-28	1.03E-24	32.75817
Nr2f1	18.25376	3.52E-20	1.55E-16	2.057193
Ebf1	16.97099	2.03E-18	5.98E-15	2.465343
Tcf7l2	16.15972	1.68E-15	2.7E-12	2.280319
Ebf3	16.08967	4.84E-18	1.07E-14	2.429213
Vim	15.97195	2.71E-18	6.82E-15	2.06231
Rpl7	14.37115	5.41E-15	6.36E-12	0.945302
Nhlh2	13.89431	2.31E-15	3.13E-12	2.147537
Barhl2	13.36624	7.58E-16	1.34E-12	2.107711
Lhx2	13.34695	3.47E-14	3.06E-11	1.813185
Tpt1	12.8143	8.18E-14	6.87E-11	1.247123
Ube2c	12.6677	8.12E-15	8.43E-12	3.084001
Eef1a1	12.51484	5.14E-13	2.92E-10	0.735164
Cnn3	12.31295	2.22E-13	1.53E-10	1.492037
Hbb-y	12.02595	6.73E-13	3.71E-10	2.678972
Hes5	11.98529	2.35E-14	2.3E-11	2.46236
Nde1	11.89173	1.99E-13	1.53E-10	3.535015
Cenpa	11.33605	2.39E-12	1.03E-09	2.477243
Crabp2	11.30777	1.06E-12	5.33E-10	2.162725
H1f0	11.29994	2.84E-12	1.19E-09	1.297954
Ccna2	11.19255	3.76E-13	2.29E-10	2.551879
Tcf12	10.87684	5.83E-12	2.06E-09	1.267464
Ddah2	10.81243	6.38E-12	2.16E-09	1.406031
Rps9	10.79055	3.73E-11	1.03E-08	0.941671
Rps11	10.77306	1.56E-11	4.58E-09	0.989904
Sdcbp	10.61393	2.32E-12	1.02E-09	1.072293
Hmgb2	10.567	7.26E-13	3.88E-10	2.281737

Table S11. Differential gene expression in subsets of cells

	Lhx9 cells KO-unique	Glut-GABA KO-unique
0	Mira	Cldn3
1	Bnc2	Mira
2	Ptger4	Tfap2a
3	Hba-x	Rnf207
4	Hoxa3	Vwa1
5	Hoxc6	Hoxa5
6	Hbb-y	Hmx1
7	Meis2	Hoxb3
8	Lpar3	Shox2
9	Dmrt2	Dmbx1
10	Stac2	Hoxc13
11	Trim71	Hoxc8
12	Hoxd11	Spint1
13	Ebf3	Tfap2b
14	Hoxa11os	Ptchd4
15	Tbx15	Rpp25
16	Hoxc9	Skor1
17	Wt1	Mab21l2
18	En1	Ndp
19	Hmx1	Cdkn2b
20	Hoxc8	Stac2
21	Tlx3	Hoxb13
22	Skor1	Lamp5
23	Slc26a10	Pax2
24	Foxf1	Hoxd11
25	Barhl2	Crabp1
26	Hbb-bh1	Hoxa7
27	Hoxb5	Tal1
28	Tal1	Pax8
29	Hoxa9	Sst
30	Hoxb2	Gata3
31	Robo3	9230102O04Rik
32	Nms	Syndig1l
33	Hoxa10	Col9a3
34	Gm26688	Hoxd10
35	Hoxd9	Fbxo27
36	Hoxc10	Hoxa10